



Published in final edited form as:

Nature. 2015 September 24; 525(7570): 528–532. doi:10.1038/nature15367.

Neutrophil ageing is regulated by the microbiome

Dachuan Zhang^{1,2}, Grace Chen^{1,2}, Deepa Manwani⁴, Arthur Mortha^{5,6}, Chunliang Xu^{1,2}, Jeremiah J. Faith^{6,7}, Robert D. Burk⁴, Yuya Kunisaki^{1,2,8}, Jung-Eun Jang^{1,2}, Christoph Scheiermann^{1,2,8}, Miriam Merad^{5,6}, and Paul S. Frenette^{1,2,3}

¹Ruth L. and David S. Gottesman Institute for Stem Cell and Regenerative Medicine Research, Albert Einstein College of Medicine, Bronx, NY 10461, USA

²Department of Cell Biology, Albert Einstein College of Medicine, Bronx, NY 10461, USA

³Department of Medicine, Albert Einstein College of Medicine, Bronx, NY 10461, USA

⁴Department of Pediatrics, Albert Einstein College of Medicine, Bronx, NY 10461, USA

⁵Department of Oncological Sciences, Mount Sinai School of Medicine, New York, NY 10029, USA

⁶The Immunology Institute, Mount Sinai School of Medicine, New York, NY 10029, USA

⁷The Institute for Genomics and Multiscale Biology, Mount Sinai School of Medicine, New York, NY 10029, USA

Abstract

Blood polymorphonuclear neutrophils provide immune protection against pathogens but also may promote tissue injury in inflammatory diseases^{1,2}. Although neutrophils are generally considered as a relatively homogeneous population, evidence for heterogeneity is emerging^{3,4}. Under steady-state conditions, neutrophil heterogeneity may arise from ageing and the replenishment by newly released neutrophils from the bone marrow⁵. Aged neutrophils up-regulate CXCR4, a receptor allowing their clearance in the bone marrow^{6,7}, with feedback inhibition of neutrophil production via the IL17/G-CSF axis⁸, and rhythmic modulation of the haematopoietic stem cell niche⁵. The aged subset also expresses low levels of L-selectin (CD62L)^{5,9}. Previous studies have suggested that *in vitro*-aged neutrophils exhibit impaired migration and reduced pro-inflammatory

Users may view, print, copy, and download text and data-mine the content in such documents, for the purposes of academic research, subject always to the full Conditions of use:http://www.nature.com/authors/editorial_policies/license.html#terms

Correspondence and requests for materials should be addressed to paul.frenette@einstein.yu.edu.

⁸Present address: Department of Medicine and Biosystemic Science, Kyushu University, Fukuoka, Fukuoka 812-8582, Japan (Y.K.); Walter Brendel Centre of Experimental Medicine, Ludwig-Maximilians-University, 81377 Munich, Germany (C.S.).

AUTHOR CONTRIBUTIONS

D.Z. designed and performed experiments, analysed results and wrote the manuscript; G.C., C.X., Y.K., R.B. and J.J. performed experiments and provided valuable inputs on the manuscript; A.M. provided *LysM-cre/Myd88^{fl/fl}* and *Csf2^{-/-}* mice and performed experiments; J.J.F. provided germ-free mice and performed experiments; D.M. provided human samples; C.S. and M.M. discussed data and provided valuable input on the manuscript; P.S.F. designed and supervised the study, discussed data and wrote the manuscript.

The authors declare no competing financial interests.

ACCESSION CODES

Gene Expression Omnibus
GSE69886

properties^{6,10}. Here, we show using *in vivo* ageing analyses that the neutrophil pro-inflammatory activity correlates positively with their ageing in the circulation. Aged neutrophils represent an overly active subset exhibiting enhanced $\alpha_M\beta_2$ integrin (Mac-1) activation and neutrophil extracellular trap (NET) formation under inflammatory conditions. Neutrophil ageing is driven by the microbiota via Toll-like receptors (TLRs)- and myeloid differentiation factor 88 (Myd88)-mediated signalling pathways. Depletion of the microbiota significantly reduces the number of circulating aged neutrophils and dramatically improves the pathogenesis and inflammation-related organ damage in models of sickle cell disease or endotoxin-induced septic shock. These results thus identify an unprecedented role for the microbiota in regulating a disease-promoting neutrophil subset.

Neutrophils are a critical component of the innate immunity. However, activated neutrophils can also promote certain diseases by secreting pro-inflammatory cytokines, and by interacting with other immune or blood cells². For example, activation of Mac-1 integrin enables adherent neutrophils to interact with platelets and red blood cells (RBCs)¹¹. In sickle cell disease (SCD), a severe blood disorder originating from a single mutation in the β -globin gene¹², the capture of sickle RBCs (sRBCs) by activated Mac-1 on adherent neutrophils leads to acute vaso-occlusion, resulting in life-threatening crises^{11,13,14}. Intravital microscopy analyses have revealed considerable heterogeneity in Mac-1 activation on neutrophils recruited to the same venules of SCD mice, suggesting that subsets of neutrophils differ markedly in their pro-inflammatory activity¹¹.

To investigate whether the heterogeneity in pro-inflammatory activity of neutrophils is associated with their ageing, we first validated that neutrophils progressively lost CD62L expression and up-regulated CXCR4 as they aged in the circulation⁵ (Extended data Fig. 1a, b). We analysed CD62L^{lo} neutrophils *in vivo* using multi-channel fluorescence intravital microscopy (MFIM) analyses^{11,13}. Interestingly, CD62L expression on adherent neutrophils in tumour necrosis factor- α (TNF- α)-inflamed post-capillary venules inversely correlated with Mac-1 activation (Fig. 1a, b), as determined by fluorescent microsphere beads that specifically bound to activated Mac-1¹¹. In addition, a similar inverse correlation was observed in the ability of adherent neutrophils to capture RBCs (Fig. 1b).

Next, we analysed neutrophil populations in mice lacking P-selectin (*Selp*^{-/-}), an adhesion molecule essential for neutrophil recruitment under steady-state conditions^{5,15}. We found that the CD62L^{lo}CXCR4^{hi} aged neutrophil population was dramatically expanded in *Selp*^{-/-} mice, and neutrophils harvested from *Selp*^{-/-} mice showed significantly higher Mac-1 activity compared to those harvested from wild-type (WT) mice (Fig. 1c, Extended data Fig. 1c, d). In addition, we analysed neutrophil populations after depletion of macrophages—which mediate neutrophil clearance¹⁶—using animals expressing the diphtheria toxin (DT) receptor knocked in the *Cd169* locus (*CD169-DTR*)¹⁷. We found that the aged neutrophil population was significantly expanded without elevation of major inflammatory cytokines, and Mac-1 activation was significantly increased on adherent neutrophils in macrophage-depleted mice (Fig. 1d, Extended data Fig. 1e, f). These data suggest that CD62L^{lo}CXCR4^{hi} aged neutrophils exhibit enhanced Mac-1 activation during inflammation.

To evaluate the specificities of ageing versus the activation of an inflammatory program, we compared the transcriptome of control, aged and TNF- α -activated neutrophils. We transfused whole blood and harvested donor neutrophils 6 h later to derive *in vivo*-aged neutrophils, and compared them to control neutrophils that were transferred for only 10 min. Additionally, we harvested neutrophils from TNF- α -treated mice for comparison with neutrophils activated by systemic inflammation. Gene set enrichment analyses¹⁸ revealed that aged neutrophils differed from activated neutrophils in many aspects, such as cytokine and chemokine secretion, Ras and P38/MAPK signalling pathways (Fig. 1e). However, aged neutrophils up-regulated several pathways that were also enhanced during neutrophil activation, including integrin and leukocyte adhesion, TLR and NOD-like receptor (NLR), and NF κ B signalling pathways (Fig. 1e, f, Extended Data Table 1,2). Analysis of surface antigens revealed that aged neutrophils exhibited significantly higher levels of TLR4 and molecules involved in cell migration and intercellular interactions, including CD11b, CD49d, and ICAM-1 (Fig. 1g, Extended data Fig. 1g–i). These results demonstrate that neutrophils constitutively receive priming signals and become more active as they age in the circulation.

The up-regulation of several inflammatory pathways in aged neutrophils suggests a contribution by exogenous inflammatory mediators. Microbiota-derived molecules may cross the intestinal barrier to exert systemic influences, affecting multiple immune populations including T cells, innate lymphoid cells (ILCs) and macrophages^{19,20}. Recent studies suggest that neutrophil production and the phagocytic capacity of bone marrow (BM)-derived neutrophils may be regulated by the microbiota^{21–24}, raising the possibility that these factors also influence the ageing process of circulating neutrophils.

We sought to test this hypothesis by treating mice with broad-spectrum antibiotics (ABX) for 4 – 6 weeks^{19,23}, which led to a highly efficient depletion and dramatic alterations in the composition of the gut microbiota (Extended data Fig. 2a–d). Microbiota depletion resulted in significant and selective reductions of neutrophil numbers in the circulation and BM, and a significant reduction in spleen cellularity with decreased numbers of multiple leukocyte populations (Extended data Fig. 3a–d). Interestingly, both the percentages and numbers of aged neutrophils were significantly reduced in ABX-treated mice, and the numbers were completely restored when the TLR4 ligand lipopolysaccharide (LPS) was added back by intragastric gavage (Fig. 2a). We further analysed neutrophil-LPS interaction by administering fluorescently labelled LPS, and found that as soon as 1 h after LPS gavage, specific fluorescence signals were detectable on neutrophils in the circulation, spleen and BM (Extended data Fig. 3e). In addition, we found that the add-back of the TLR2 ligand peptidoglycan (PGN), but not the NOD1/2 activator mTriDAP, could also restore the numbers of aged neutrophils in ABX-treated mice (Extended data Fig. 3f), suggesting that multiple microbiota-derived molecules may contribute to neutrophil ageing under steady state.

To validate that the microbiota could indeed regulate neutrophil ageing, we analysed neutrophil populations in germ-free (GF) mice. Compared to specific pathogen-free (SPF) animals, GF mice exhibited broad alterations in both innate and adaptive immune cells (Extended data Fig. 4a–c). Consistently, the numbers of total and aged neutrophils were

significantly reduced in GF mice, and the numbers were partially restored when GF mice were reconstituted by fecal transplantation. In addition, treating GF mice with ABX did not further reduce their aged neutrophil numbers (Fig. 2b, Extended data Fig. 4d, e). Furthermore, we transfused whole blood obtained from WT donor mice into WT, ABX-treated or GF recipients. The percentages of chronologically aged donor neutrophils progressively increased after the transfusion, but at a significantly slower rate in ABX-treated and GF recipients (Fig. 2c). These results strongly suggest that neutrophil ageing is delayed in a bacterially depleted environment.

Since alternations in neutrophil clearance may influence the number of aged neutrophils (Fig. 1c, d), we investigated whether ABX treatment modulates neutrophil ageing by acting on clearance mechanisms. We first analysed adhesion molecule expression on endothelial cells and observed no difference between control and ABX-treated mice (Extended data Fig. 5a). Next, we analysed macrophage numbers in the spleen, BM and liver, the organs that clear neutrophils²⁵. We found that macrophage numbers decreased by ~36% in the spleen, increased by ~30% in the BM, and did not change in the liver of ABX-treated mice (Extended data Fig. 5b, c). Furthermore, we depleted macrophages in ABX-treated mice using the *CD169-DTR* model, and found that ABX treatment significantly reduced aged neutrophil numbers in macrophage-depleted animals (Extended data Fig. 5c, d), suggesting that microbiota-driven ageing and macrophage-mediated clearance are independent mechanisms that regulate the number of aged neutrophils. We then analysed the release-clearance kinetics of circulating neutrophils using EdU pulse-chase labelling strategy¹⁶. We observed significantly more EdU⁺ neutrophils remaining in the circulation on day 7, suggesting a delayed clearance in ABX-treated mice (Fig. 2d). In addition, we investigated the functional impact of microbiota depletion using intravital microscopy, and observed significant reductions in neutrophil adhesion and Mac-1 activation in ABX-treated compared to control mice (Fig. 2e–g). These data suggest that neutrophil ageing, which leads to the generation of a functionally overly active subset of neutrophils, is driven by the microbiota.

Neutrophils express multiple pattern recognition receptors, including TLR2 and TLR4²⁶, which may directly transduce microbiota-derived signals. Alternatively, microbiota-derived signals may stimulate certain immune cells to secrete pro-inflammatory cytokines such as TNF- α and GM-CSF^{19,27}, which could in turn prime circulating neutrophils. To investigate how microbiota-derived signals regulate neutrophil ageing, we characterized aged neutrophils in *LysM-cre/Myd88^{fl/fl}* mice, in which Myd88, a signalling molecule that mediates most TLR signalling, is specifically deleted in myeloid cells. Interestingly, we observed significant reductions in the percentages and numbers of aged neutrophils in these mice (Fig. 3a, Extended data Fig. 5e). Similarly, we also found significant reductions of aged neutrophils in TLR2 and TLR4 knockout mice (Extended data Fig. 5f). By contrast, the aged neutrophil population was expanded in TNF- α and GM-CSF knockout mice (Fig. 3b, Extended data Fig. 5g), arguing that the microbiota may not drive neutrophil ageing by stimulating TNF- α or GM-CSF secretion.

To further delineate how Myd88 mediates microbiota-driven ageing, we adoptively transferred either *LysM-cre/Myd88^{fl/fl}* or WT neutrophils into WT or *LysM-cre/Myd88^{fl/fl}*

recipient mice, and analysed donor neutrophil ageing *in vivo*. Interestingly, neutrophil ageing was almost completely abrogated when Myd88-deficient neutrophils were transferred into WT recipients, whereas the ageing kinetics remained largely unaffected when WT neutrophils were transferred into *LysM-cre/Myd88^{fl/fl}* recipients (Fig. 3c). Next, we generated chimeric mice reconstituted with a mixture of WT and Myd88-, TLR4- or TLR2-deficient BM cells, which enabled us to compare WT and deficient neutrophils in the same mouse, thus avoiding potential differences caused by the environment. Consistently, we observed significantly lower percentages of the aged subset in Myd88-, TLR2- and TLR4-deficient neutrophils, compared to WT neutrophils in the same chimeric mice (Fig. 3d). By contrast, the percentages of total neutrophils in Myd88-, TLR2- and TLR4-deficient leukocytes were unaltered or expanded (Extended data Fig. 5h), suggesting a specific effect of TLR and Myd88 deficiency on ageing, but not the generation, of neutrophils. We also subjected these chimeric mice to intravital microscopy, and found significantly lower Mac-1 activity on Myd88-, TLR4- and TLR2-deficient neutrophils (Fig. 3e, f, Extended data Fig. 5i). These findings strongly suggest that neutrophil TLRs and Myd88 signalling mediate microbiota-driven neutrophil ageing.

In addition to analysing Mac-1 activation, we investigated whether ageing affects the ability of neutrophils to form NETs in response to pathological stimulation. We enriched aged neutrophils by injecting antibodies to block P- and E-selectins⁵, and found that neutrophils harvested from anti-selectin-treated mice exhibited significantly increased reactive oxygen species (ROS) production (Extended data Fig. 6a, b). We induced NET formation by treating neutrophils with LPS *in vitro*²⁸, and quantified NETs based on the co-localization of DNA with citrullinated histone H3 (CitH3) and neutrophil elastase (NE)²⁹. We found that NET formation was significantly increased in neutrophils harvested from anti-selectin-treated mice. By contrast, neutrophils isolated from ABX-treated mice exhibited a marked reduction in NET formation (Extended data Fig. 6c, d).

To investigate whether microbiota depletion impacts NET formation *in vivo*, we challenged control and ABX-treated mice with a lethal dose of LPS to induce septic shock¹⁵, and injected fluorophore-conjugated antibodies to image NETs in the liver vasculature. Strikingly, we observed a significant reduction in the number of NETs formed in septic liver after microbiota depletion, and dramatic decreases in soluble NET biomarkers—plasma nucleosome and plasma DNA (Extended data Fig. 7a, b). In addition, immunofluorescence analyses revealed that the septic liver vasculature contained numerous aggregated CitH3⁺ neutrophils, which was commonly found to be associated with fibrin deposition (Extended data Fig. 7c, d). By contrast, CitH3⁺ neutrophils, neutrophil aggregates and fibrin deposition were markedly reduced in ABX-treated mice, leading to significantly prolonged survival of these mice (Extended data Fig. 7c–g). Remarkably, this improvement in survival was abrogated by infusing *aged* neutrophils, but not by infusing same numbers of *young* neutrophils back into ABX-treated mice (Extended data Fig. 7g).

To assess further the role of neutrophil ageing in a disease model, we analysed mice with SCD, a disease characterized by recurrent episodes of vaso-occlusion in which neutrophils play a primary function^{11,14}. While SCD mice exhibited significant expansion of all major leukocyte subsets compared to hemizygous (SA) mice, ABX-mediated microbiota depletion

led to a significant and selective reduction of neutrophils, but not other leukocyte populations (Extended data Fig. 8a). Strikingly, aged neutrophils were expanded by >10-fold in SCD mice, and the expansion was completely abrogated by microbiota depletion (Fig. 4a).

To investigate the functional impact of reduced aged neutrophil numbers in disease outcome, we challenged SA, untreated and ABX-treated SCD mice with TNF- α and evaluated the cremaster microcirculation by intravital microscopy^{11,14}. SCD mice exhibited significant increases in neutrophil adhesion, Mac-1 activation and heterotypic interactions with RBCs compared to SA mice, all of which were markedly reduced by microbiota depletion (Fig. 4b, c, Extended data Fig. 8b, c), resulting in enhanced blood flow and significantly improved survival of ABX-treated SCD mice (Fig. 4d). Most interestingly, the splenomegaly of SCD mice was significantly reduced, and liver damage including fibrosis, necrosis and inflammation was dramatically alleviated in ABX-treated SCD mice (Fig. 4e, f, Extended data Fig. 8d, e). To test the impact of impaired neutrophil clearance in SCD, we depleted macrophages in the liver, spleen and BM using clodronate liposome¹⁷. Macrophage depletion markedly increased circulating aged neutrophils (data not shown) and resulted in acute vaso-occlusive crises that led to the death of all mice within 10 – 30 h (Fig. 4g). Together, these data suggest that the microbiota regulates aged neutrophil numbers, thereby affecting both acute vaso-occlusive crisis and the ensuing chronic tissue damage in SCD.

Finally, we evaluated whether the numbers of circulating aged neutrophils were altered in patients with SCD. As Penicillin V antibiotic prophylaxis therapy is recommended for children < 5 years or older patients with immune defects to prevent life-threatening infections³⁰, we determined aged neutrophil numbers in this patient population (Extended data Fig. 8f, g). While there was no significant difference in total neutrophil numbers between SCD patients and healthy subjects, patients in the Penicillin V prophylaxis group had significantly lower total neutrophil numbers (Fig. 4h). Consistent with our results in the mouse model, we found that SCD patients exhibited a marked increase in the numbers of circulating aged neutrophils compared to healthy controls. Remarkably, we observed significant reductions in both percentages and numbers of aged neutrophils in patients on Penicillin V prophylaxis compared with SCD patients not taking antibiotics (Fig. 4h, Extended data Fig. 8f). Age differences, gender or hydroxyurea intake in this case-control study did not mitigate the effect of antibiotic treatment on aged neutrophil numbers (Extended data Fig. 8h), although a prospective study with age-matched subjects will be needed to ascertain the independent value of antibiotics in controlling aged neutrophil numbers in SCD.

Neutrophils are among the shortest-lived cells in the body¹. However, the evolutionary forces behind their rapid turn-over remain unclear. Our results suggest that signals from the microbiota, through TLRs and Myd88, gradually lead them to become more functionally active. These data thus emphasize the notion that the immunity is maintained by a balanced activation resulting from encounters with the microbiota, and bring a possible explanation for the evolutionary pressure for keeping an energy-consuming short lifespan as a mechanism to fine-tune the proportion of highly active neutrophils while balancing the risk of tissue injury. To our knowledge, this is the first therapy shown to alleviate the chronic

tissue damage induced by SCD. Although antibiotic therapy normalised the overly active aged neutrophil population in SCD patients, the extent of which this treatment affects the gut microbiota or vaso-occlusive disease is open to future investigations. Our results raise the possibility that manipulation of the microbiome may have sustained implications in disease outcome that should be further studied in clinical trials.

METHODS

Mice

Selp^{-/-}, *CD169-DTR*, *Csf2*^{-/-} mice, Tg[Hu-miniLCR α 1^{G γ A γ δ β S}] *Hba*^{-/-} *Hbb*^{-/-} (Berkeley sickle cell mice) and Tg[Hu-miniLCR α 1^{G γ A γ δ β S}] *Hba*^{-/-} *Hbb*^{+/-} (hemizygous control mice) have been described^{11,14,17,19}. B6.129P2-*Lyz2*^{tm1(cre)lfo/J} (*LysM-Cre*), B6.129P2(SJL)-*Myd88*^{tm1Defr/J} (*Myd88*^{fl/fl}) and B6;129S-*Tnf*^{tm1Gkl/J} (*Tnf*^{-/-}) mice were purchased from The Jackson Laboratory. *Tlr2*^{-/-} and *Tlr4*^{-/-} mice were kindly provided by Dr. Eric G. Pamer (Memorial Sloan-Kettering Cancer Center, NY). C57BL/6 CD45.1 and CD45.2 mice were purchased from the National Cancer Institute. Six to eight week old mice were used for experiments. All mice were housed in specific pathogen-free conditions and fed with autoclaved food, and experimental procedures performed on mice were approved by the Animal Care and Use Committee of Albert Einstein College of Medicine. Germ-free C57/BL6 mice were maintained in sterile isolators with autoclaved food and water in the Gnotobiotic Core of Icahn School of Medicine at Mount Sinai. For fecal transplantation experiments, 100 mg of feces pellets was resuspended in 1 ml of PBS, homogenized, and filtered through a 70 μ m strainer. Recipient GF mice were gavaged with 200 μ l of the filtrate.

Human samples

Blood was obtained from healthy volunteers, SCD patients and SCD patients on penicillin V prophylaxis after parental consent and child assent as approved by the Institutional Review Board of Albert Einstein College of Medicine. SCD patients were recruited upon routine visits at the sickle cell clinic of Montefiore Medical Center. Among the 34 patients recruited for the study, 11 were on Penicillin V due to age of <5 or defective immunity, and 23 were off antibiotic treatment for at least 2 months. Patients with acute infection or vaso-occlusive crisis were excluded from the study.

Bone marrow transplantation

Age- and gender-matched sickle cell disease (SS) and control hemizygous (SA) mouse cohorts were generated by transplanting bone marrow (BM) nucleated cells from Berkeley sickle cell mice or control hemizygous mice into lethally irradiated C57BL/6 mice as described before^{11,14}. Fully reconstituted mice (> 97%) were used for studies. Chimeric mice used to study neutrophil TLRs were generated by transplanting a 1:1 mixture of BM nucleated cells from C57BL/6 mice (CD45.1⁺) and *LysM-cre/Myd88*^{fl/fl} or *Tlr4*^{-/-} or *Tlr2*^{-/-} mice (CD45.2⁺) into lethally irradiated C57BL/6 recipients (CD45.1⁺). Chimeric mice were analysed 6 weeks after transplantation.

Antibiotic treatment

WT or SCD mice were treated with Ampicillin (1g/L), Streptomycin (1g/L), Metronidazol (1g/L) and Vancomycin (1g/L) in drinking water for 4 – 6 weeks. Antibiotics were purchased from Sigma or Jack D. Weiler Hospital of the Albert Einstein College of Medicine. Drinking water containing antibiotics was changed every 3 – 4 days. For microbial product add-back experiment, ABX-treated WT mice were fed with 1 mg LPS (O111:B4, Sigma), 1 mg Peptidoglycan (PGN-SA, Invivogen) or 1mg MurNAc-L-Ala- γ -D-Glu-mDAP (M-TriDAP) by intragastric gavage, and allowed to rest for 24 – 36 h. For the analysis of neutrophil-LPS interaction, untreated WT mice were fed with 300 μ g LPS-FITC (Sigma) by intragastric gavage, and tissues were harvested 1 hour after gavage.

Adoptive transfer

For *in vivo* neutrophil ageing analysis, whole blood from donor mice was transfused into recipient mice by retro-orbital injection. Donor neutrophils in blood were tracked based on CD45.1 and CD45.2 expression by flow cytometry. For microarray analyses, control and aged neutrophils were derived by *in vivo* ageing for 10 min and 6 h, respectively. Activated neutrophils were harvested from mice injected with 0.5 μ g TNF- α (R&D Systems) for 2 hours. To analyse Mac-1 activation of neutrophils from WT and *Selp*^{-/-} mice, 3–5 \times 10⁶ leukocytes were harvested from blood following red blood cell (RBC) lysis, and were labelled with red fluorescent dye PKH26 (Sigma) according to the manufacturer's protocol before the transfer into recipient mice.

Macrophage depletion

For the depletion of CD169⁺ macrophages, WT or *CD169-DTR* mice were injected intraperitoneally with two doses of 10 μ g/kg body weight diphtheria toxin (Sigma) three days apart. Mice were analysed five days after the second injection. For depletion of macrophages in SCD mice, mice were injected intravenously with 250 μ l PBS- or clodronate-encapsulated liposomes (the Foundation Clodronate Liposomes) as described before¹⁷.

Flow cytometry and cell sorting

Cells were surface-stained in PEB buffer (PBS supplemented with 0.5% BSA and 2mM EDTA) for 20–30 min on ice. Multiparametric flow cytometric analyses were performed on a LSRII equipped with FACS Diva 6.1 software (BD Biosciences) and analysed with FlowJo software (Tree Star). Dead cells were excluded by FSC, SSC and 4',6-diamino-2-phenylindole (DAPI, Sigma) staining. Cell sorting experiments were performed on Aria Cell Sorter (BD Biosciences). Neutrophils were gated by Gr-1^{hi} CD115^{lo} SSC^{hi}; T cells, B cells and monocytes were gated by CD3⁺, CD4⁺ and CD115^{hi}; aged neutrophils were gated by CD62L^{lo} CXCR4^{hi} within the neutrophil population; hematopoietic progenitor and stem cells were identified by lineage cocktail, Sca-1, KitL, CD150, CD48, CD34 and CD16/32, as previously described³¹; macrophages were identified by Gr-1^{lo} CD115^{lo} F4/80⁺ SSC^{lo} as previously described¹⁷. Fluorophore-conjugated or biotinylated antibodies against mouse Gr-1 (RB6-8C5), CD115 (AFS98), CD3 (145-2C11), B220 (RA3-6B2), PE-anti-CXCR4 (2B11), CD45.1 (A20), CD45.2 (104), CD11b (M1/70), ICAM-1 (YN1/1.7.4), CD11c (N418), CD49d (R1-2), CD45 (30-F11), Sca-1 (D7), c-kit (2B8), CD34 (RAM34), and

F4/80 (BM8) were from eBioscience. Antibodies specific to CD62L (MEL-14) and Biotin Mouse Lineage Panel (TER-119, RB6-8C5, RA3-6B2, M1/70, 145-2C11) were from BD Pharmingen. Antibodies against CD47 (miap301), CD150 (TC15-12F12.2), CD48 (HM48-1) and CD16/32 (93) were from BioLegend.

Blood leukocyte counts

Blood was harvested from the retro-orbital plexus, collected in EDTA or heparin, and analysed on ADVIA 120 hematology system (SIEMENS).

Brightfield intravital microscopy

Experimental procedures and data analyses were performed as previously described^{11,13,14}. Briefly, male mice were injected intrascrotally with 0.5 µg TNF-α (R&D Systems), and were anesthetized 2 h later by intraperitoneal injection of a mixture of 2% chloralose (Sigma) and 10% urethane (Sigma) in PBS. Tracheal intubation was performed to ensure normal respiration after anesthesia. The cremaster muscle was gently exteriorized, and mounted onto a microscopic stage, and then superfused with Ringer solution (pH 7.4, 37°C). Under the microscope, leukocyte rolling, adhesion, transmigration and neutrophil-RBC interactions in post-capillary venules (20 – 40 µm in diameter) were captured using a custom-designed upright microscope (MM-40, Nikon) equipped with a 60X water immersion objective (Nikon). Adhesion was quantified as the number of leukocytes remaining stationary for more than 20s within a 100 µm venular segment. In this model, more than 90% of adherent leukocytes are neutrophils based on previous studies¹³. Neutrophil-RBC interactions were defined as the associations between an RBC and an adherent leukocyte for more than 3 seconds, and quantified as the number of interactions within a 100µm vessel segment per minute. At least 8 vessels from each animal were recorded and analysed using a charge-coupled video camera (Hamamatsu) and video recorder (Sony SVHS, SVO-9500). Venular diameters were measured using a video caliper, and centerline red cell velocity (V_{RBC}) for each venule recorded was measured using an optical Doppler velocimeter (Texas A&M). Blood flow rate (Q) was calculated as $Q = V_{mean} \times \pi d^2/4$, where d is venule diameter, V_{mean} is estimated as $V_{RBC}/1.6$.

Multi-channel fluorescence intravital microscopy (MFIM)

MFIM analyses of Mac-1 activation of adherent neutrophils were performed as previously described¹¹. Briefly, yellow-green fluorescent microsphere beads (FMB, 1.0 µm, Life technologies) were incubated with 1 mg/ml bovine serum albumin (BSA, Fisher Bioreagents) for at least 2 h in PBS and sonicated for 15 min in a water-bath sonicator (Laboratory Supplies Co.). Albumin-coated beads (10^9 beads/mouse) were injected into mice prepared for intravital microscopy 3 h after TNF-α injection. For measurement of CD62L expression on adherent neutrophils, mice were intravenously injected with 4 µg APC-anti-CD62L (clone MEL-14, BD Pharmingen). For *in vivo* staining of CD45 alleles, mice were intravenously injected with 5 – 10 µg Alexa Fluor 647-anti-CD45.2 (clone 104, Biolegend) and biotin-anti-CD45.1 (clone A20, eBioscience), and 20 min later injected with 5 – 10 µg streptavidin eFluor 450 (eBioscience). Images and videos were captured using an Axio Examiner.D1 microscope (Zeiss) equipped with a Yokogawa CSU-X1 confocal scan

head with four stack laser system (405nm, 488nm, 561nm, and 642nm wavelengths) and a 60X water immersion objective, and analysed using Slidebook software (Intelligent Imaging Innovations). Mac-1 activation of adherent neutrophils was quantified as the average number of beads captured by each adherent neutrophil in post-capillary venules, and the percentage of cells that captured more than 8 beads.

Intravital microscopic studies of SCD mice

Male mice were injected intraperitoneally with 0.5 µg TNF-α (R&D Systems), and 2 h later neutrophil responses were analysed as described above. Survival times, defined as the time from TNF-α injection until death, were recorded.

Microarray analysis

Total RNA from 2000 sorted neutrophils was extracted using RNeasy Plus Micro Kit (Qiagen) according to the manufacturer's protocol. All further steps were performed at the Genomics Core Facility at Albert Einstein College of Medicine. RNA was amplified using Ovation One-Direct System (NuGEN). Amplified cRNA was labelled with the GeneChip WT terminal labelling kit (Affymetrix), hybridized to Mouse Gene ST 1.0 microarrays (Affymetrix), and scanned by GeneChip Scanner 3000 7G system (Affymetrix) according to standard protocols. Raw data were normalized by RMA algorithm and analysed using the Gene Pattern analysis platform (Broad Institute). After removal of unannotated genes, gene set enrichment analysis was performed with all C2 gene sets from the Molecular Signatures Database (v4.0, Broad Institute). Gene sets with p-value of < 0.05 in either aged or activated groups were considered to have significant differences compared to control group. Normalized enrichment score (NES) for selected pathways related to neutrophil functions were depicted as a heat map, with gene sets clustered by functional classifications.

Quantitative real-time PCR (Q-PCR)

Messenger RNA extraction from 500 – 2000 sorted neutrophils using Dynabeads mRNA DIRECT™ Kit (Life technologies) and reverse transcription using RNA to cDNA EcoDry Premix (Clontech) were performed according to the manufacturer's protocols. Q-PCR was performed with SYBR GREEN (Roche) on ABI PRISM 7900HT Sequence Detection System (Life technologies). The PCR protocol started with one cycle at 95 °C (10 min) and continued with 40 cycles at 95 °C (15 s) and 60 °C (1 min). Expression of glyceraldehyde-3-phosphate dehydrogenase (*Gapdh*) was used as a standard. The average threshold cycle number (Ct) for each tested gene was used to quantify the relative expression of each gene: $2^{[Ct(\text{standard}) - Ct(\text{gene})]}$. Primers include:

Gapdh forward: TGTGTCCGTCGTGGATCTGA

Gapdh reverse: CCTGCTTCACCACCTTCTTGA

Tlr4 forward: ATGGCATGGCTTACACCACC

Tlr4 reverse: GAGGCCAATTTTGTCTCCACA

Icam1 forward: GGACCACGGAGCCAATTC

Icam1 reverse: CTCGGAGACATTAGAGAACAATGC

Itgam forward: CTGAACATCCCATGACCTTCC

Itgam reverse: GCCCAAGGACATATTCACAGC

Cxcl2 forward: CGCTGTCAATGCCTGAAG

Cxcl2 reverse: GGCGTCACACTCAAGCTCT

ELISA

Concentrations of IFN- γ , IL6, TNF- α and IL1 β were measured in plasma from WT and *CD169-DTR* mice 5 days after DT treatment using ELISA kits (eBioscience) according to the manufacturer's instructions. For measurement of NET biomarkers, plasma nucleosome was measured using Cell Death Detection ELISA Plus kit (Roche), and plasma DNA was measured using Sytox Green (Life technologies) as previously described²⁹.

16S rDNA quantification

Stool pellets were collected and total DNA was extracted using the QIAamp Fast DNA Stool Mini Kit (Qiagen). Quantification of 16S rDNA was performed by real-time q-PCR using TaqMan® Universal Master Mix (Life technologies) and the following primers and probe as described³²: Fwd 5'-ACTGAGAYACGGYCCA-3', Rev 5'-TTACCGCGGCTGCTGGC-3', Probe 6-FAM-ACTCCTACGGGAGGCAGCAGT-BHQ1.

Taxonomic microbiota analysis

Taxonomic microbiota analysis was performed by the Molecular Biology and Next Generation Technology Core at Albert Einstein College of Medicine. In simple, purified 16S rDNA was used for PCR amplification and sequencing. The variable region 4–6 (V4-V6) of the 16S rDNA gene was amplified using barcoded 16V6R1052 and 16SV4F515 primers. Sequencing was performed using paired-end Illumina MiSeq sequencing. Taxonomical classification was obtained using the RDP-classifier to generate an OTU table, and the percentage of each family-genus in total microbiome was derived from the OTU values.

Neutrophil release-clearance kinetics

Mice were injected intraperitoneally with 2 mg EdU and were bled on day 2 – 7 after EdU injection. Each mouse was bled only once to avoid the potential change in kinetics caused by bleeding. Cells were surface stained, fixed with 2% paraformaldehyde (PFA), and permeabilized with 0.1% Triton-X. After permeabilization, EdU incorporation was detected by Click-iT EdU Alexa Fluor 647 Imaging Kit (Life technologies) according to the manufacturer's instructions.

In vitro NET assay

Circulating neutrophils were harvested using Percoll Density Centrifugation Media (GE Healthcare) as previously described²⁹. Briefly, blood was loaded onto a Percoll gradient consisting of 52%, 65% and 78% Percoll layers, and centrifuged at 2500 rpm for 30 min at room temperature. The cell bands between 65% and 78% layers were harvested, and RBCs were removed using RBC lysis buffer. Purity of 80 – 95% was constantly achieved with this method, as analysed by flow cytometry. For ROS production assay, neutrophils were treated

with 20 µg/ml LPS (0111:B4, Sigma) for 30 min. ROS detection was performed using fluorogenic dye Dihydrorhodamine 123 (Life technologies) as previously described³³. For NET formation *in vitro*, neutrophils were attached to poly-L-lysine coated slides and treated with 20 µg/ml LPS (0111:B4, Sigma) for 3 h. Following stimulation, cells were stained without fixation with SYTOX Orange (cell impermeable) and SYTO 13 (cell permeable) nucleic acid dyes (Life technologies) to image DNA fibres and distinguish live and dead cells. After DNA staining, cells were fixed, permeabilized and blocked as previously described²⁹. Cells were incubated with goat anti-neutrophil elastase (sc-9521, Santa Cruz Biotechnology) and rabbit anti-CitH3 (ab5103, Abcam) followed by Alexa Fluor 647 Donkey-anti-goat (Life technologies) and Brilliant Violet 421 donkey anti-rabbit (Biolegend) secondary antibodies. Species-matching isotype controls were used to confirm fluorescence staining. NETs were defined by DNA fibres co-localized with NE and CitH3 proteins with a length exceeding 40 µm, and quantified as the percentage of NETs among all neutrophils present in the field.

***In vivo* NET assay**

For analyses of NET formation *in vivo*, goat anti-neutrophil elastase (sc-9521, Santa Cruz Biotechnology), and rabbit anti-CitH3 (ab5103, Abcam) were labelled by APEX Alexa Fluor 647 and APEX Alexa Fluor 568 antibody labelling kit (Life technologies), respectively, according to the manufacturer's instructions. Mice were injected intraperitoneally with 30 mg/kg LPS for 3 h, and then were injected intravenously with 5 µg Alexa Fluor 568-labelled anti-CitH3, 2 µg Alexa Fluor 647-labelled anti-NE, 10 µg Pacific Blue-anti-CD31 (clone 390 or clone MEC13.3, Biolegend) and 10 µM SYTOX Green (cell impermeable) nucleic acid dye (Life technologies). Species-matching isotype controls were also labelled using the same protocol and injected into septic mice to validate fluorescence staining. Fresh livers were harvested 20 min after antibody injections, and directly imaged using Axio Examiner.D1 confocal microscope (Zeiss). Confocal microscopy visualized with a penetration of ~100 µm into the tissue. Liver vasculature was identified by CD31 staining. NETs were defined by extracellular DNA fibres stained by SYTOX Green, anti-CitH3 and anti-NE antibodies with a length exceeding 40 µm, and quantified as the average number of NETs in each vessel.

Immunofluorescence

Tissues were embedded in Tissue-Plus O.C.T. Compound (Fisher HealthCare), and frozen sections of 20 µm thick were prepared using CM3050 S cryostat (Leica). Sections were fixed with 4% PFA for 10 min, and blocked and permeabilised with PBS containing 20% species-matching serum and 0.5% Triton-X for 1 – 2 hours. Adhesion molecules on endothelial cells were stained by PE-anti-P-selectin (clone Psel.KO2.3, eBioscience), PE-anti-E-selectin (clone 10E9.6, BD Pharmingen), PE-anti-ICAM-1 (clone YN1/1.7.4, eBioscience), and PE-anti-VCAM-1 (clone 429, Biolegend). Expression of adhesion molecules was quantified using Slidebook software (Intelligent Imaging Innovations) as previously described¹⁵. For immunofluorescence staining of neutrophils on sections, goat anti-neutrophil elastase (sc-9521, Santa Cruz Biotechnology) and rabbit anti-CitH3 (ab5103, Abcam) were used, followed by Alexa Fluor 568 Donkey-anti-goat and Alexa Fluor 488 donkey anti-rabbit (Life technologies) secondary antibodies. For analyses of fibrin

deposition, sections were fixed using formalin containing 2% acetic acid for 30 min to remove soluble fibrinogen and leave only cross-linked fibrin in the tissue³⁴. Sections were then blocked and permeabilised, and incubated with goat anti-Fibrinogen β (sc-18029, Santa Cruz Biotechnology) and PE-anti-Ly6G (clone 1A8, biolegend), followed by Alexa Fluor 568 Donkey-anti-goat secondary antibody (Life Technologies). In all immunofluorescence experiments, endothelial cells were identified by Alexa Fluor 647-anti-CD31 (MEC13.3, Biolegend) and nuclei were stained by Hoechst 33342 (Life Technologies).

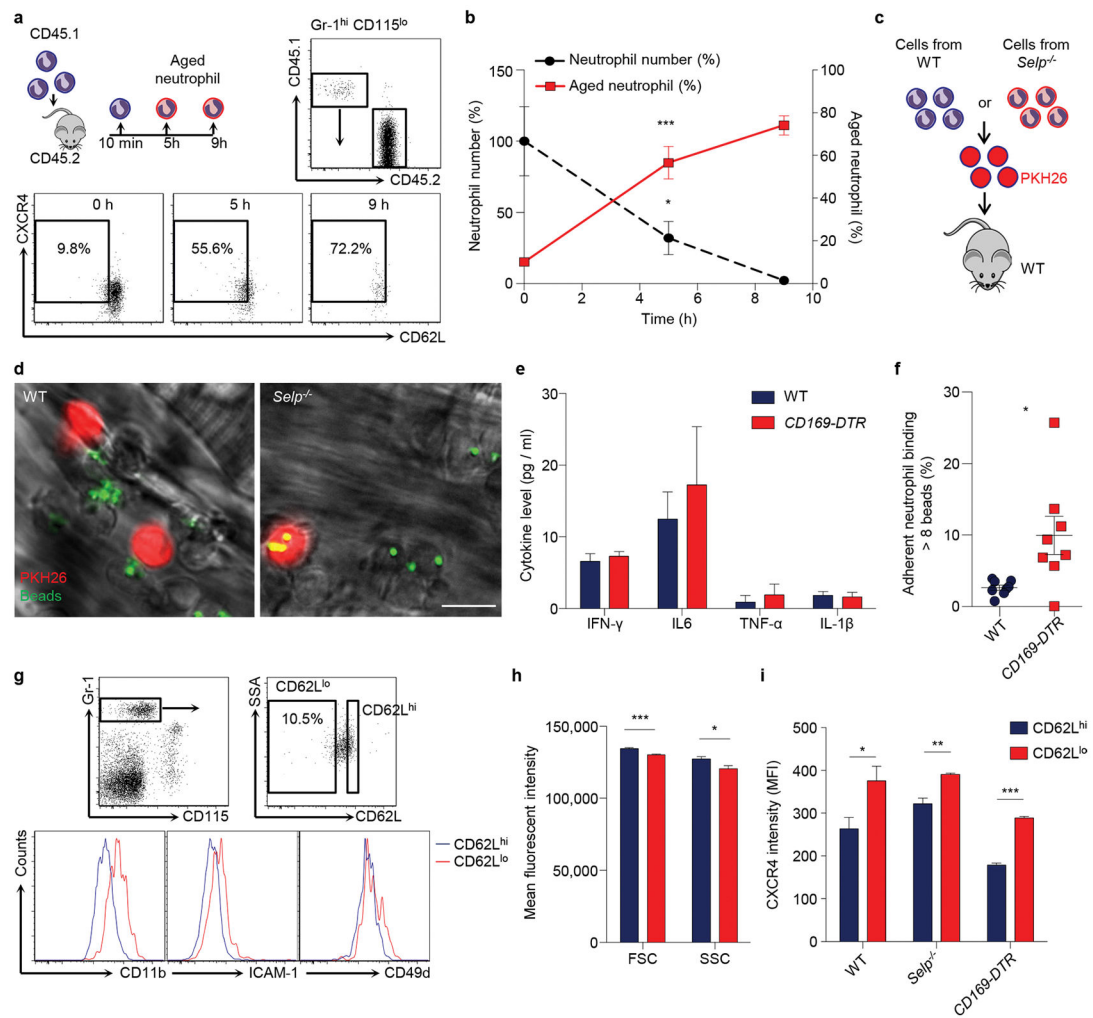
Histology analyses of septic mice

Mice were injected intraperitoneally with 30 mg/kg LPS, and livers were harvested 24 h after injection and fixed in 10% formalin. Histological analyses were performed by the Histology and Comparative Pathology Facility at Albert Einstein College of Medicine according to standard protocols. Survival time was defined as the time from LPS injection until death of the mouse and recorded with a maximum of 150 h.

Statistical analysis

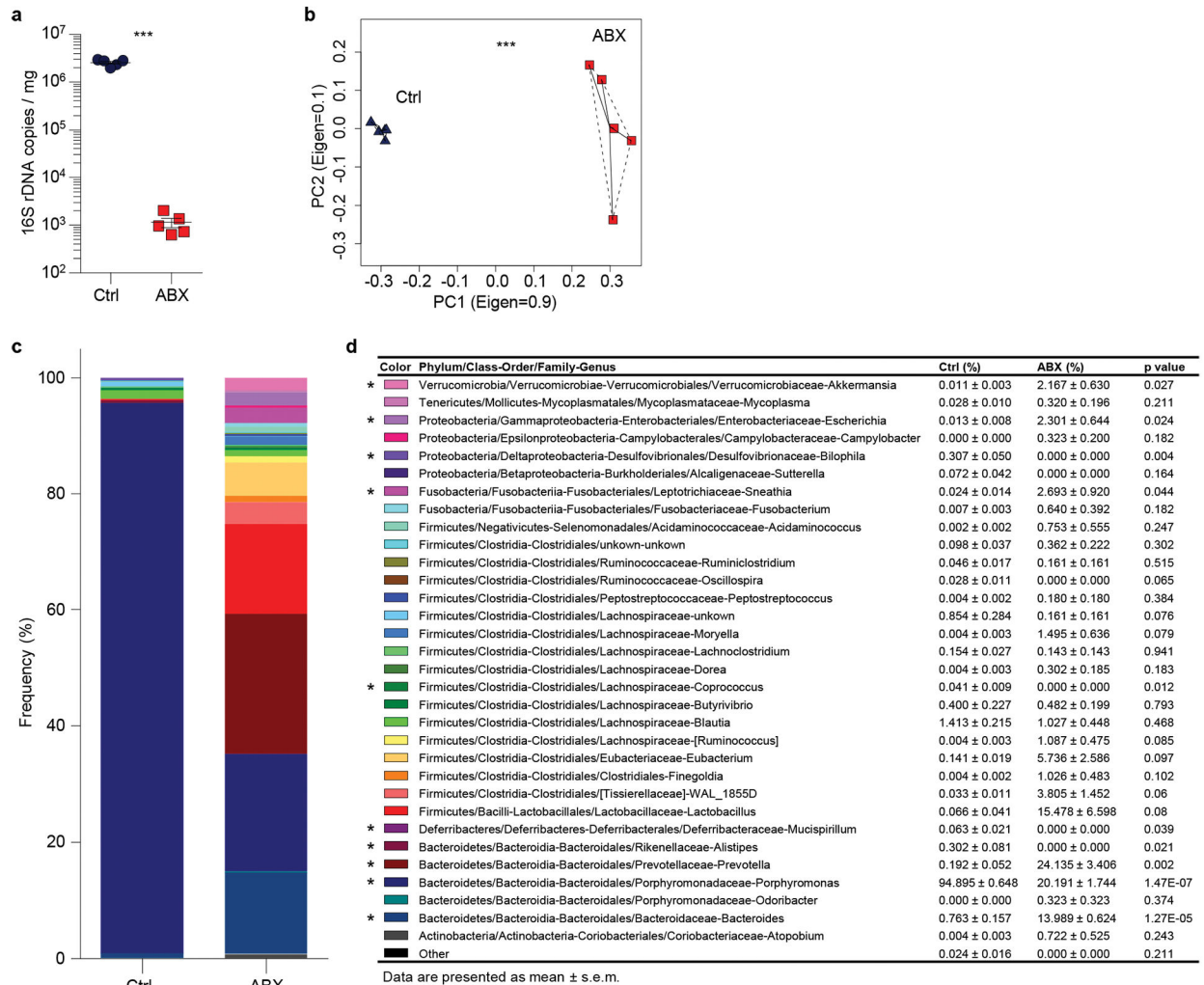
No statistical methods were used to predetermine the sample size. Experiments were performed blind to group allocations, and validated by two investigators independently. Paired and unpaired two-sided Student's *t*-tests and *Mann-Whitney* test were used to compare two groups. One-way *ANOVA* analysis was used for multiple group comparisons. *Log-rank* test was used to compare survival curves. Statistical analyses were performed using Graph Pad Prism 6 software.

Extended Data

**Extended Data Figure 1. Phenotypic and functional characterization of aged neutrophils**

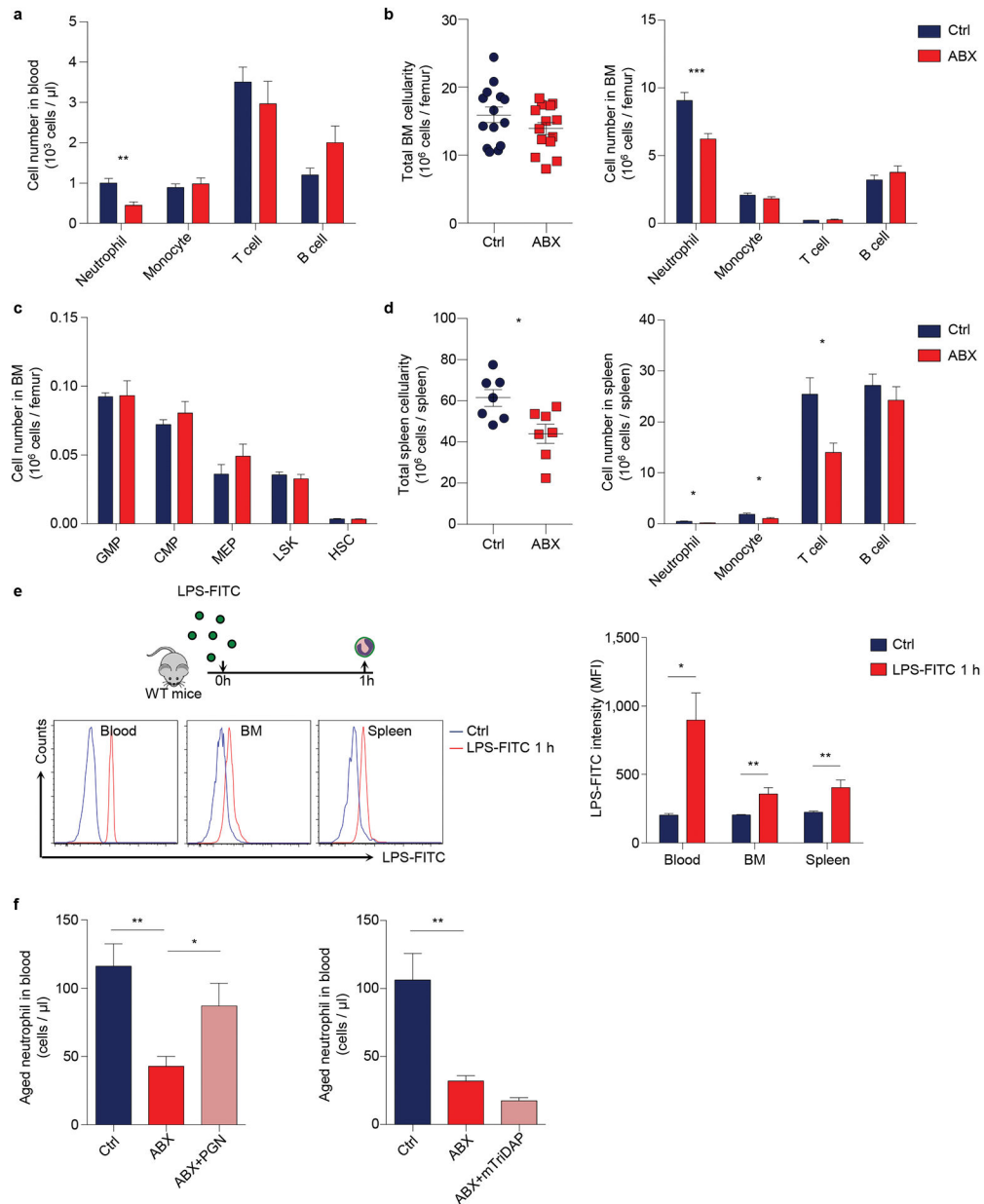
a, Flow cytometry analysis of donor neutrophil ageing after adoptive transfer into recipients. Donor neutrophils gated by CD45.1⁺ and aged neutrophils gated by CD62L^{lo}CXCR4^{hi}. **b**, Ageing and clearance kinetics of donor neutrophils after adoptive transfer into recipients (n = 3 mice). Left y-axis, donor neutrophil number relative to the initial number of neutrophils transferred (black dash line); right y-axis, percentage of the aged subset in donor neutrophils (red line). **c–d**, MFIM analysis of Mac-1 activation of neutrophils harvested from WT or *Selp*^{-/-} mice, labelled by PKH26 (red) and transferred into WT recipients. Scale bar, 10 μm. **e**, Plasma cytokine levels in WT and *CD169-DTR* mice 5 days after DT treatment (n = 5 mice). **f**, Percentages of adherent neutrophils that capture > 8 beads in diphtheria toxin (DT)-treated WT and *CD169-DTR* mice (n = 8 mice). **g–h**, Flow cytometry analysis of surface marker expressions (**g**), cell size (FSC) and granularity (SSC; **h**; n = 7 mice) on CD62L^{hi} young and CD62L^{lo} aged neutrophils. **i**, CXCR4 expression levels on CD62L^{hi} young and CD62L^{lo} aged neutrophils in WT, *Selp*^{-/-}, and *CD169-DTR* mice (WT: n = 13 mice; *Selp*^{-/-}: n = 4 mice; *CD169-DTR*: n = 5 mice). Error bars, mean ± s.e.m. * *P* < 0.05, ** *P* <

0.01, *** $P < 0.001$, data representing 2 independent experiments analysed with one-way ANOVA (b) or unpaired Student's t -test (e-i).



Extended Data Figure 2. Antibiotic treatment efficiently depletes and alters the composition of the microbiota

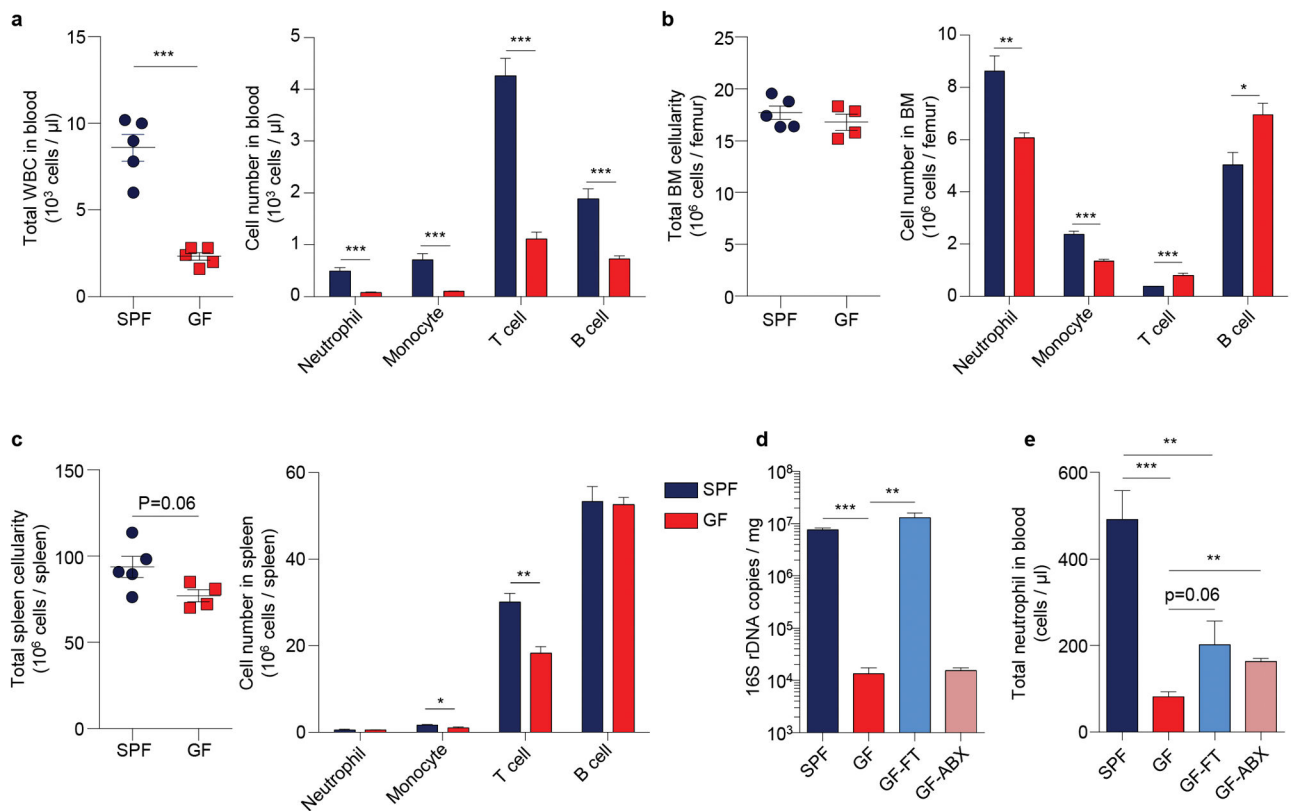
a, Copy numbers of 16S ribosomal DNA in feces from control and antibiotics (ABX)-treated mice ($n = 5$ mice). **b**, Principal component analysis of the microbiome composition in control and ABX-treated mice ($n = 5$ mice). **c-d**, Percentage of each bacteria genus in total microbiome ($n = 5$ mice). Error bars, mean ± s.e.m. * $P < 0.05$, *** $P < 0.001$, data representing 2 independent experiments analysed with unpaired Student's t -test (**a**, **d**) or permutational multivariate ANOVA (**b**).



Extended Data Figure 3. Microbiota-derived molecules regulate neutrophil homeostasis and ageing

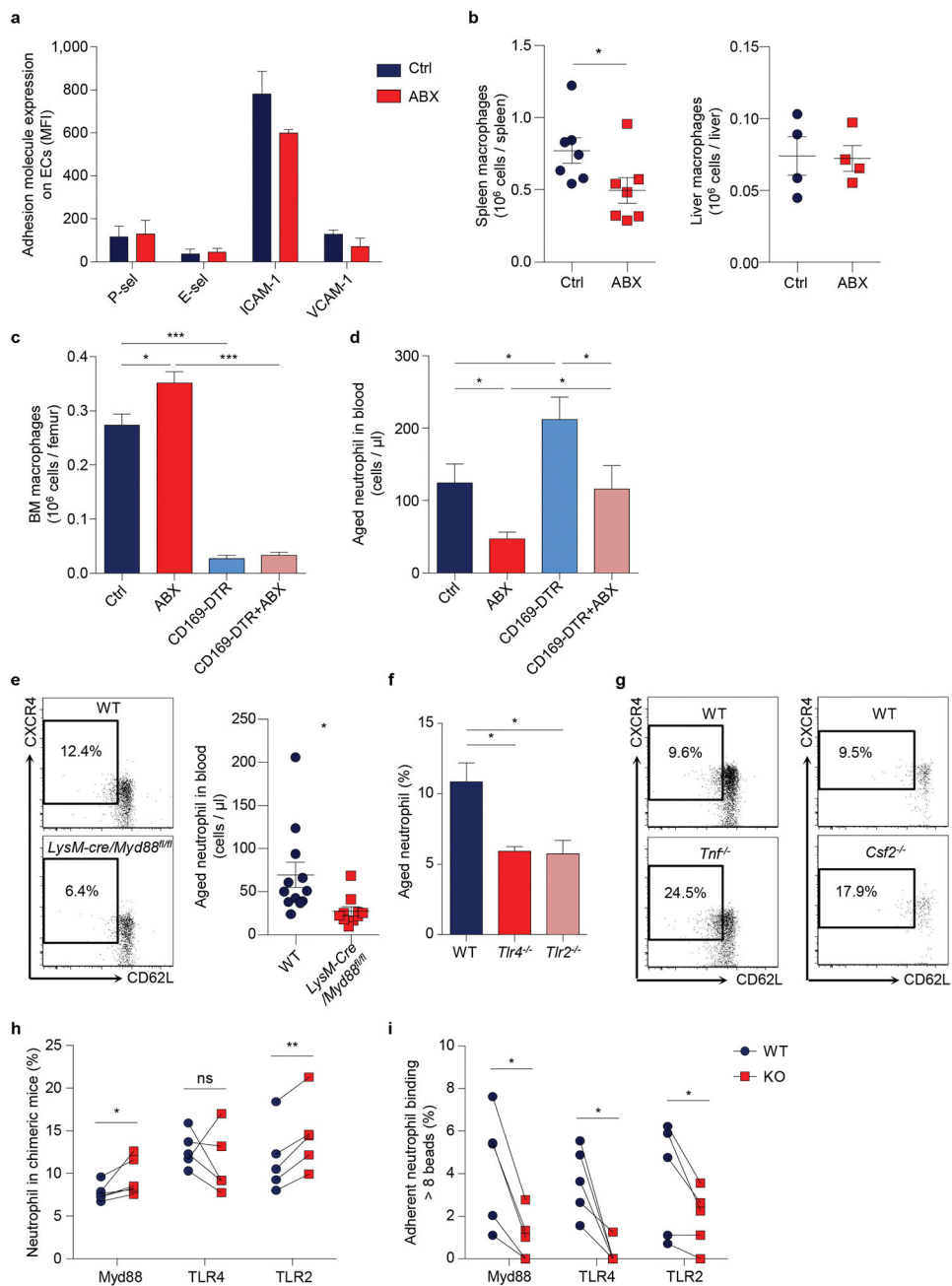
a, Numbers of circulating leukocyte subsets in control and antibiotics (ABX)-treated mice ($n = 9$ mice). **b**, Bone marrow cellularity and numbers of leukocyte subsets in the bone marrow of control and ABX-treated mice ($n = 14$ mice). **c**, Numbers of bone marrow hematopoietic stem and progenitor cells in control and ABX-treated mice ($n = 9$ mice). **d**, Spleen cellularity and numbers of leukocyte subsets in the spleen of control and ABX-treated mice ($n = 7$ mice). **e**, Flow cytometry analysis of neutrophil-LPS interactions in blood, bone marrow and spleen 1 hour after LPS-FITC gavage (Ctrl: $n = 4$ mice; LPS-FITC: $n = 5$ mice). Histogram showing fluorescence intensity on neutrophils gated by Gr-1^{hi} CD115^{lo} SSA^{hi}. **f**, Numbers of circulating aged neutrophils in control, ABX-treated, and ABX-treated mice fed

with peptidoglycan (PGN) or mTriDAP (left, $n = 11,9,9$ mice; right, $n = 10,10,5$ mice). Error bars, mean \pm s.e.m. * $P < 0.05$, ** $P < 0.01$, *** $P < 0.001$, data representing 2 independent experiments analysed with unpaired Student's t -test.



Extended Data Figure 4. Neutrophil homeostasis is altered in germ-free mice

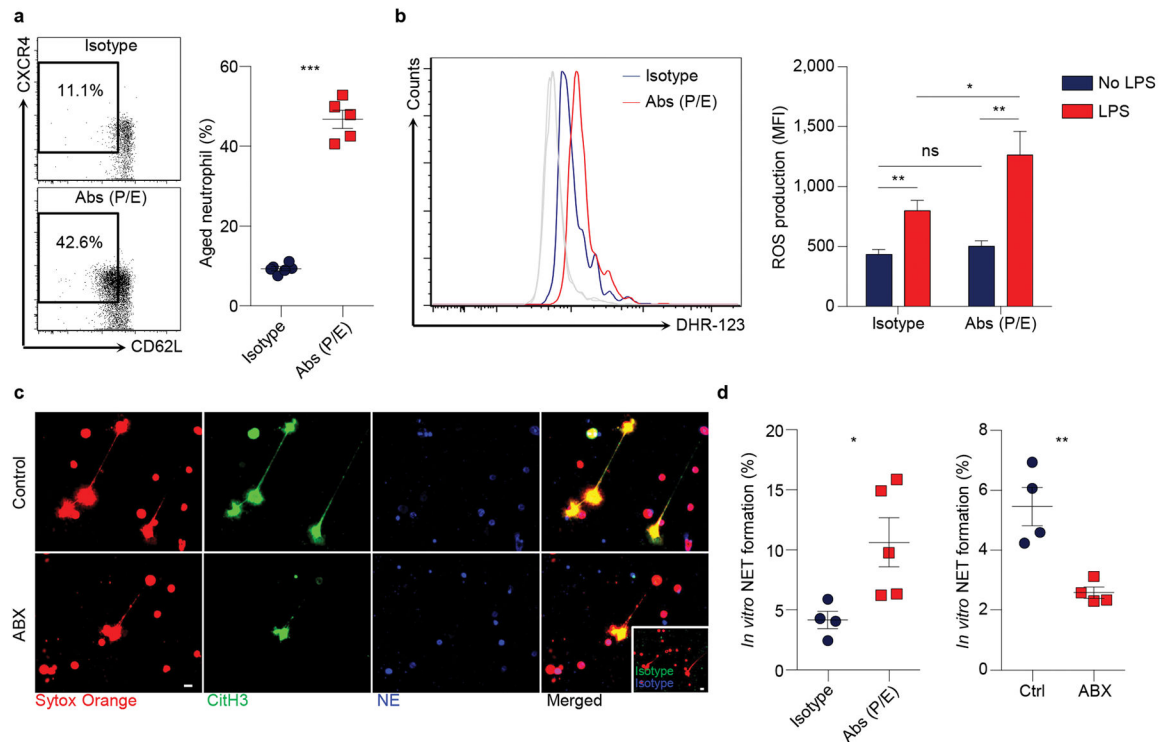
a, Total WBC counts and numbers of leukocyte subsets in blood of specific pathogen free (SPF) and germ-free (GF) mice ($n = 5$ mice). **b**, Total BM cellularity and numbers of leukocyte subsets in the BM of SPF and GF mice (SPF: $n = 5$ mice; GF: $n = 4$ mice). **c**, Total spleen cellularity and numbers of leukocyte subsets in the spleen of SPF and GF mice (SPF: $n = 5$ mice; GF: $n = 4$ mice). **d**, Copy numbers of 16S ribosomal DNA in feces from SPF mice, GF mice, GF mice reconstituted by fecal transplantation (GF-FT), and antibiotics-treated GF mice (GF-ABX; $n = 5,5,5,4$ mice). **e**, Numbers of total circulating neutrophils in SPF, GF, GF-FT, and GF-ABX mice ($n = 5,5,5,3$ mice). Error bars, mean \pm s.e.m. * $P < 0.05$, ** $P < 0.01$, *** $P < 0.001$, data representing 2 independent experiments analysed with unpaired Student's t -test.



Extended Data Figure 5. Microbiota-driven neutrophil ageing is independent of clearance mechanisms, and mediated by TLRs and Myd88 signalling

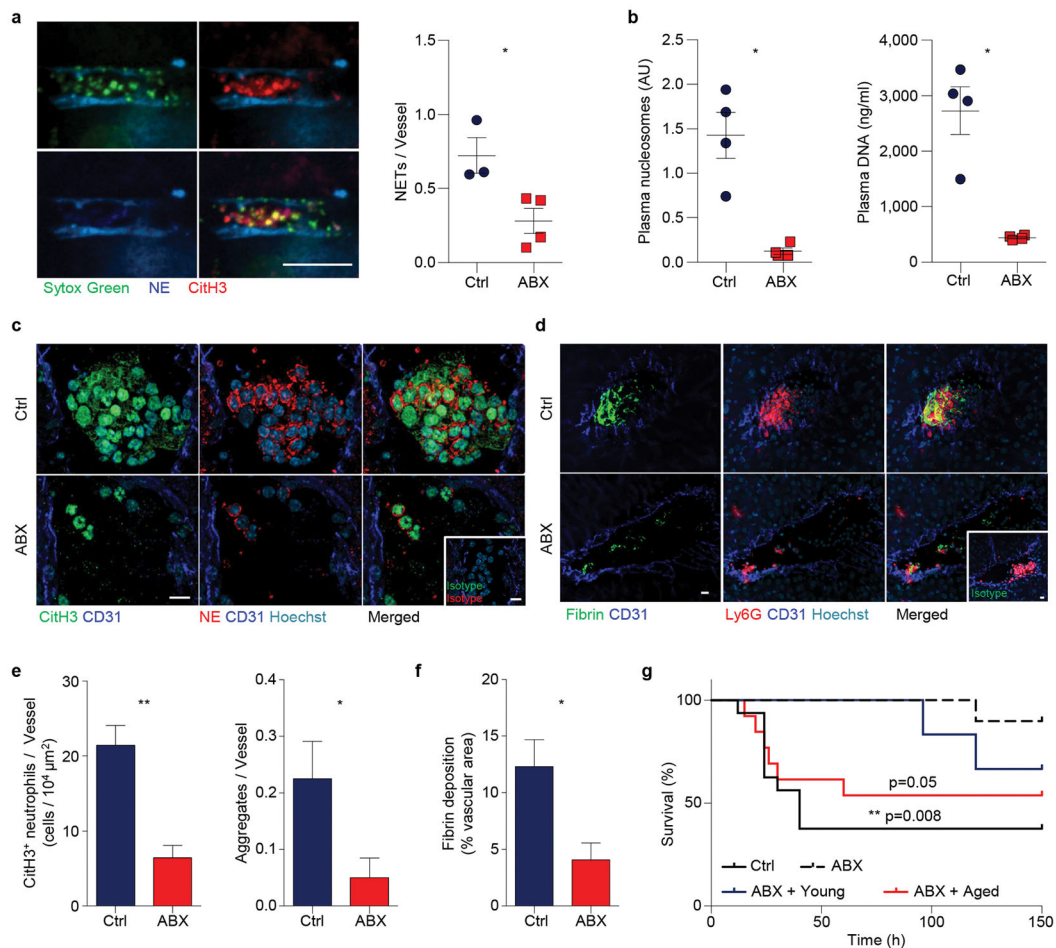
a, Adhesion molecule expression on endothelial cells in control and antibiotics (ABX)-treated mice (n = 4 mice). **b**, Numbers of spleen, and liver macrophages in control and ABX-treated mice (left, n = 7 mice; right, n = 4 mice). **c-d**, Numbers of BM macrophages (**c**; n = 19,19,10,10 mice) and circulating aged neutrophils (**d**; n = 12,11,10,9 mice) in diphtheria toxin (DT)-treated control, ABX-treated mice, *CD169-DTR*, and ABX-treated *CD169-DTR* mice. **e**, Flow cytometry analysis of aged neutrophils in WT and *LysM-cre/Myd88^{fl/fl}* mice (n = 12,10 mice). **f**, Percentages of aged neutrophils in WT, *Tlr4^{-/-}* and

Tlr2^{-/-} mice (n = 10,10,12 mice). **g**, Flow cytometry analysis of aged neutrophils in WT and *Tnf*^{-/-} or *Csf2*^{-/-} mice. **h**, Percentages of WT and *LysM-cre/Myd88*^{fl/fl} or *Tlr4*^{-/-} or *Tlr2*^{-/-} neutrophils in total leukocyte population in chimeric mice (n = 5 mice). **i**, Percentages of WT and *LysM-cre/Myd88*^{fl/fl} or *Tlr4*^{-/-} or *Tlr2*^{-/-} neutrophils that capture > 8 beads in chimeric mice (n = 5 mice). Error bars, mean ± s.e.m. * *P* < 0.05, ** *P* < 0.01, *** *P* < 0.001, data representing 2 independent experiments analysed with unpaired Student's *t*-test (**a–f**) or paired Student's *t*-test (**h, i**).



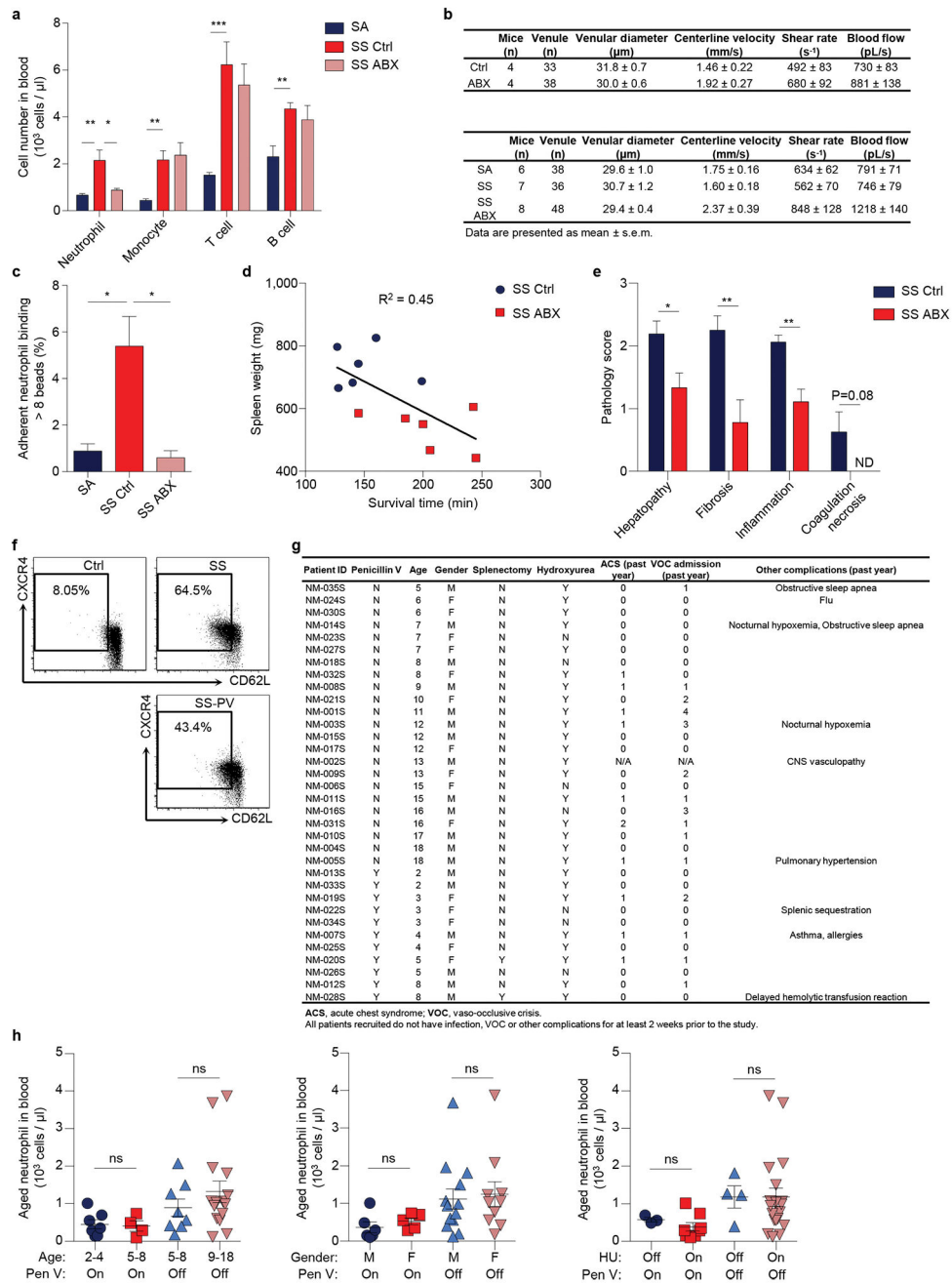
Extended Data Figure 6. Microbiota depletion inhibits NET formation

a, Flow cytometry analysis of aged neutrophils in isotype and anti-P/E-selectin antibody-treated mice (n = 6,5 mice). **b**, ROS production of neutrophils from isotype and anti-P/E-selectin antibody-treated mice, as analysed by flow cytometry using Dihydrorhodamine 123 (DHR-123; Isotype: n = 10; Abs (P/E): n = 11 mice). Grey lines, background fluorescence of neutrophils from both groups without LPS stimulation. **c**, LPS-induced NET formation of neutrophils from control and antibiotics (ABX)-treated mice, as analysed by immunofluorescence staining of DNA (sytox orange), neutrophil elastase (NE) and citrullinated histone 3 (CitH3). Inset, isotype control. Scale bars, 10 μm. **d**, Quantification of NET formation of neutrophils from isotype and anti-P/E-selectin antibody-treated mice, or from control and ABX-treated mice (left, n = 4,5 mice; right, n = 4 mice). Error bars, mean ± s.e.m. * *P* < 0.05, ** *P* < 0.01, *** *P* < 0.001, data representing 2 independent experiments analysed with unpaired Student's *t*-test.



Extended Data Figure 7. Microbiota depletion benefits endotoxin-induced septic shock

a, Representative images and quantification of *in vivo* NET formation in liver vasculature of control and antibiotics (ABX)-treated mice challenged with 30mg/kg LPS (n = 3,4 mice). Scale bar, 10 μm. **b**, Quantification of NET biomarkers, plasma nucleosome and DNA, in septic control and ABX-treated animals (n = 4 mice). **c–d**, Representative images showing CitH3⁺ neutrophil aggregates (**c**) and fibrin deposition associated with neutrophil aggregates (**d**) in septic liver of control and ABX-treated mice. Arrows, diffusive CitH3 and NE proteins. Insets, isotype controls. Scale bars, 10 μm. **e–f**, Numbers of CitH3⁺ neutrophils and neutrophil aggregates (**e**; left: n = 4 mice; right: n = 40 vessels from 4 mice) and quantification of fibrin deposition (**f**; n = 4,3 mice) in septic liver of control and ABX-treated mice. **g**, Survival time of control, ABX-treated mice, and ABX-treated mice infused with 2×10⁶ aged or young neutrophils in septic shock induced by 30mg/kg LPS (n = 16,10,13,6 mice). Error bars, mean ± s.e.m. * *P* < 0.05, ** *P* < 0.01, data representing 2 independent experiments analysed with unpaired Student's *t*-test (**a**, **e**(left), **f**), *Mann-Whitney* test (**b**, **e**(right)) or *Log-rank* test (**g**).



Extended Data Figure 8. Microbiota depletion affects disease progression in sickle cell disease

a, Numbers of circulating leukocyte subsets in hemizygous control (SA), control SCD (SS Ctrl) and antibiotics-treated SCD (SS ABX) mice (SA: n = 8 mice; SS Ctrl: n = 9 mice; SS ABX: n = 9 mice). **b**, Hemodynamic parameters of mice analysed for neutrophil adhesion and integrin activation. **c**, Percentages of adherent neutrophils that capture > 8 beads in SA, SS Ctrl and SS ABX mice (n = 4,3,3 mice). **d**, Correlation between the survival times of SS ctrl and SS ABX mice in acute vaso-occlusive crisis and their spleen weights. R square = 0.45. **e**, Scoring of liver damage, liver fibrosis, inflammation and necrosis in SS Ctrl and SS ABX (n = 8,9 mice). **f**, Flow cytometry analysis of aged neutrophils in healthy controls,

SCD patients (SS), and SCD patients on penicillin V prophylaxis (SS-PV). **g**, Demographics of human subjects analysed for aged neutrophil numbers. **h**, Aged neutrophil numbers in SCD patients grouped by age, gender, hydroxyurea (HU) and penicillin V (Pen V) treatment (Ctrl: n = 9 subjects; SS: n = 23 subjects; SS-PV: n = 11 subjects). Error bars, mean \pm s.e.m. * $P < 0.05$, ** $P < 0.01$, *** $P < 0.001$, data representing 2 independent experiments analysed with unpaired Student's *t*-test (**a**, **c**, **h**) or *Mann-Whitney* test (**e**).

Extended Data Table 1

Pathways selected for the analysis of neutrophil functions.

Pathway	Gene set name
Innate immune system	REACTOME_INNATE_IMMUNE_SYSTEM
Local acute inflammatory response	BIOCARTA_LAIR_PATHWAY
Leukocyte adhesion and diapedesis	BIOCARTA_LYM_PATHWAY
MAPK signaling for integrins	REACTOME_P130CAS_LINKAGE_TO_MAPK_SIGNALING_FOR_INTEGRINS
Cell surface integrin pathway	PID_INTEGRIN_CS_PATHWAY
Fc-gamma receptor mediated phagocytosis	KEGG_FC_GAMMA_R_MEDIATED_PHAGOCYTOSIS
Lymphoid/Non-lymphoid interactions	REACTOME_IMMUNOREGULATORY_INTERACTIONS_BETWEEN_A_LYMPHOID_AND_A_NON_LYMPHOID_CELL
ROS pathway	BIOCARTA_FREE_PATHWAY
Peroxisome	KEGG_PEROXISOME
Cell/ECM interactions	REACTOME_CELL_EXTRACELLULAR_MATRIX_INTERACTIONS
Degradation of ECM	REACTOME_DEGRADATION_OF_THE_EXTRACELLULAR_MATRIX
Complement and coagulation cascades	KEGG_COMPLEMENT_AND_COAGULATION_CASCADES
TLR signaling pathway	KEGG_TOLL_LIKE_RECEPTOR_SIGNALING_PATHWAY
TLR endogenous pathway	PID_TOLL_ENDOGENOUS_PATHWAY
TLR4 signaling	REACTOME_ACTIVATED_TLR4_SIGNALLING
NLR signaling pathway	KEGG_NOD_LIKE_RECEPTOR_SIGNALING_PATHWAY
NLR pathway	REACTOME_NUCLEOTIDE_BINDING_DOMAIN_LEUCINE_RICH_REPEAT_CONTAINING_RECEPTOR_NLR_SIGNALING_PATHWAYS
NOD1/2 signaling pathway	REACTOME_NOD1_2_SIGNALING_PATHWAY
RLR pathway	KEGG_RIG_I_LIKE_RECEPTOR_SIGNALING_PATHWAY
RIG I mediated induction of IFN alpha	REACTOME_RIG_I_MDA5_MEDIATED_INDUCION_OF_IFN_ALPHA_BETA_PATHWAYS
Activation of NFkB	REACTOME_ACTIVATION_OF_NF_KAPPAB_IN_B_CELLS
NFkB canonical pathway	PID_NFKAPPABCANONICALPATHWAY
NFkB atypical pathway	PID_NFKAPPABATYPICALPATHWAY
NFkB activation by RIP1	REACTOME_IKK_COMPLEX_RECRUITMENT_MEDIATED_BY_RIP1
NFkB activation through FADD/RIP1 pathway	REACTOME_NFKB_ACTIVATION_THROUGH_FADD_RIP1_PATHWAY_MEDIATED_BY_CASPASE_8_AND10
NFkB activation by TAK1	REACTOME_TAK1_ACTIVATES_NFKB_BY_PHOSPHORYLATION_AND_ACTIVATION_OF_IKKS_COMPLEX
NFkB and MAPK activation mediated by TLR4	REACTOME_NFKB_AND_MAP_KINASES_ACTIVATION_MEDIATED_BY_TLR4_SIGNALING_REPERTOIRE
NFkB activation induced by TRAF6	REACTOME_TRAF6_MEDIATED_INDUCION_OF_NFKB_AND_MAP_KINASES_UPON_TLR7_8_OR_9_ACTIVATION
Chemokine signaling pathway	KEGG_CHEMOKINE_SIGNALING_PATHWAY
CXCR2 pathway	PID_IL8CXCR2_PATHWAY
Cytokine signaling pathway	REACTOME_CYTOKINE_SIGNALING_IN_IMMUNE_SYSTEM
Cytokines	BIOCARTA_CYTOKINE_PATHWAY
IL1 pathway	REACTOME_IL1_SIGNALING
IL2 receptor beta pathway	BIOCARTA_IL2RB_PATHWAY
IL4 pathway	ST_INTERLEUKIN_4_PATHWAY
IL6 pathway	REACTOME_IL_6_SIGNALING
IL12 pathway	PID_IL12_2PATHWAY
IL23 pathway	PID_IL23PATHWAY

Pathway	Gene set name
IL27 pathway	PID_IL27PATHWAY
IFN-alpha signaling	REACTOME_REGULATION_OF_IFNA_SIGNALING
IFN-gamma pathway	REACTOME_INTERFERON_GAMMA_SIGNALING
TNFR1 pathway	BIOCARTA_TNFR1_PATHWAY
TNF/p75/NTR signaling	PID_P75NTRPATHWAY
TNFR2 pathway	BIOCARTA_TNFR2_PATHWAY
PPAR signaling pathway	KEGG_PPAR_SIGNALING_PATHWAY
p38/MAPK pathway	REACTOME_P38MAPK_EVENTS
ERK pathway	REACTOME_SIGNALLING_TO_ERKS
PIP3 signaling pathway	SIG_PIP3_SIGNALING_IN_CARDIAC_MYOCYTES
Ras signaling pathway	REACTOME_SIGNALLING_TO_RAS
RhoA pathway	PID_RHOA_PATHWAY
HDAC Class I pathway	PID_HDAC_CLASSI_PATHWAY
G-alpha I signaling pathway	REACTOME_G_ALPHA_I_SIGNALLING_EVENTS
NFAT pathway	PID_NFAT_TFPATHWAY
PDGF pathway	BIOCARTA_PDGF_PATHWAY
Rac1 pathway	PID_RAC1_PATHWAY
AKT pathway	BIOCARTA_AKT_PATHWAY
MAPK pathway	BIOCARTA_MAPK_PATHWAY
HIF pathway	BIOCARTA_HIF_PATHWAY
Purinergic receptor signaling pathway	REACTOME_NUCLEOTIDE_LIKE_PURINERGIC_RECEPTORS
Purinergic receptor P2Y signaling pathway	REACTOME_P2Y_RECEPTORS
Translation	REACTOME_TRANSLATION
Ribosome	KEGG_RIBOSOME
43S Ribosome	REACTOME_ACTIVATION_OF_THE_MRNA_UPON_BINDING_OF_THE_CAP_BINDING_COMPLEX_AND_EIFS_AND_SUBSEQUENT_BINDING_TO_43S
EIF pathway	BIOCARTA{EIF_PATHWAY
Protein export	KEGG_PROTEIN_EXPORT
Amino acid degradation	REACTOME_METABOLISM_OF_AMINO_ACIDS_AND_DERIVATIVES
Proteasome	KEGG_PROTEASOME
Ubiquitin mediated proteolysis	KEGG_UBIQUITIN_MEDIATED_PROTEOLYSIS
Protein degradation-Parkin pathway	BIOCARTA_PARKIN_PATHWAY
Cell death	BIOCARTA_DEATH_PATHWAY
Caspase cascades	SA_CASPASE_CASCADE
Cell death mitochondria pathway	BIOCARTA_MITOCHONDRIA_PATHWAY

Gene set name refers to Molecular Signatures Database v5.0 (Broad Institute).

Extended Data Table 2

Gene set enrichment analysis of selected pathways in aged and activated neutrophils.

Category	Pathway	Aged NES	Aged p-val	Activated NES	Activated p-val
Immune Functions	Innate immune system	1.2282217	0.10245901	2.1779234	0
	Local acute inflammatory response	1.1145728	0.3392857	1.8885438	0.001930502
	Leukocyte adhesion and diapedesis	1.5105772	0.06352941	1.6552799	0.025242718
	MAPK signaling for integrins	1.4485482	0.061440676	1.6242106	0.032128513
	Cell surface integrin pathway	1.4916337	0.0675	-1.2022164	0.24557522
	Fc-gamma receptor mediated phagocytosis	0.8664476	0.6876877	1.61418	0.008116883
	Lymphoid/Non-lymphoid interactions	0.8654324	0.6196172	1.5619569	0.033557046
	ROS pathway	-0.95446336	0.5321429	1.7730503	0.005565863
	Peroxisome	-1.203138	0.20919882	1.6480244	0.003395586
	Cell/ECM interactions	-0.7654254	0.7643979	1.772366	0.006048387

Catagory	Pathway	Aged NES	Aged p-val	Activated NES	Activated p-val
	Degradation of ECM	-1.4378743	0.095914744	1.5911175	0.028462999
	Complement and coagulation cascades	-1.5144768	0.070853464	1.6505035	0.030303031
Immune Functions PRR and NFKB Signaling	TLR signaling pathway	1.4612477	0.026706232	2.3468528	0
	TLR endogenous pathway	1.3665496	0.1056338	1.5889539	0.035714287
	TLR4 signaling	1.0985918	0.31333333	1.9638056	0
	NLR signaling pathway	1.4583313	0.05479452	2.5441191	0
	NLR pathway	1.4290915	0.07730673	2.1706495	0
	NOD1/2 signaling pathway	1.3088835	0.13197969	2.2286413	0
	RLR pathway	-0.8638851	0.6666667	2.1639493	0
	RIG I mediated induction of IFN alpha	-0.8472993	0.7259843	2.0400646	0
	Activation of NFKB	1.2855691	0.11396012	1.8813537	0.001718213
	NFKB canonical pathway	1.3068268	0.1495098	2.174795	0
	NFKB atypical pathway	0.8993623	0.6034483	1.9205661	0.001949318
	NFKB activation by RIP1	1.7887179	0.002192983	1.8208189	0.001930502
	NFKB activation through FADD/RIP1 pathway	1.8454865	0.008928572	1.6110392	0.033898305
	NFKB activation by TAK1	1.2061867	0.22624435	2.0932863	0
	NFKB and MAPK activation mediated by TLR4	1.1569227	0.22841226	1.8594357	0
	NFKB activation induced by TRAF6	1.0924268	0.27714285	1.6228119	0.010016695
Immune Functions Cytokine and Chemokine	Chemokine signaling pathway	-0.7447356	0.8922652	1.433992	0.028616853
	CXCR2 pathway	-0.9767436	0.5085324	1.5124553	0.050583657
	Cytokine signaling pathway	-1.1273036	0.25921053	2.1093962	0
	Cytokines	-0.9237167	0.5686275	1.5562985	0.039325844
	IL1 pathway	1.6451061	0.02925532	2.078718	0
	IL2 receptor beta pathway	-2.0031374	0	1.2259008	0.2228261
	IL4 pathway	-1.312908	0.16470589	1.5741479	0.03169014
	IL6 pathway	-0.8152665	0.7010676	1.5760885	0.046747968
	IL12 pathway	-1.6290972	0.014240506	1.9707948	0.001675042
	IL23 pathway	-1.2130085	0.24518389	1.9758543	0
	IL27 pathway	-1.3348651	0.16555184	1.7636672	0.005464481
	IFN-alpha signaling	-0.8072854	0.68761224	1.6680452	0.014705882
	IFN-gamma pathway	1.4466043	0.087804876	2.066193	0
	TNFR1 pathway	1.2722206	0.16010499	1.6132443	0.032432433
	TNF/p75/NTR signaling	1.3214921	0.08732394	1.726003	0.003231018
	TNFR2 pathway	-0.8648928	0.6243386	1.9728887	0
Signal Pathways	PPAR signaling pathway	-0.8915187	0.6086956	2.0968451	0
	p38/MAPK pathway	-1.0720062	0.37918216	1.9020989	0
	ERK pathway	-1.1935399	0.24440895	1.4667499	0.04886562
	PIP3 signaling pathway	-1.4735942	0.05496183	1.5826265	0.022452503
	Ras signaling pathway	-1.6251277	0.02680067	1.4745739	0.07090909
	RhoA pathway	-1.6779591	0.017133957	1.1863663	0.24090122
	HDAC Class I pathway	-1.7304282	0.00608828	1.3537472	0.09764919
	G-alpha I signaling pathway	-0.8018528	0.78581977	1.4290625	0.03891709
	NFAT pathway	-1.5555012	0.039087947	-1.6272985	0.027272727
	PDGF pathway	-1.6846628	0.01983471	-1.7379107	0.014354067
	Rac1 pathway	0.64468014	0.91351354	1.5256119	0.033043478
	AKT pathway	0.95451254	0.56	1.5437053	0.05009634
	MAPK pathway	1.1132134	0.25617284	1.637257	0.003289474
	HIF pathway	1.6175048	0.03117506	1.2415975	0.24675325
	Purinergic receptor signaling pathway	1.5389258	0.06153846	1.6881694	0.015968064

Catagory	Pathway	Aged NES	Aged p-val	Activated NES	Activated p-val
	Purinergic receptor P2Y signaling pathway	1.5777047	0.036876354	1.4960046	0.0503876
Cellular Functions	Translation	1.4605397	0.028673835	-1.8208151	0
	Ribosome	1.1336436	0.23906706	-1.8144947	0
	43S Ribosome	1.1219336	0.28531855	-1.8783303	0
	EIF pathway	1.2240345	0.23933649	-1.5321815	0.05
	Protein export	1.5375326	0.06122449	-0.91629106	0.5726496
	Amino acid degradation	-1.5101556	0.018518519	1.3439316	0.05457464
	Proteosome	-1.3857354	0.06864274	1.4372953	0.06989247
	Ubiquitin mediated proteolysis	-0.926711	0.593361	1.7934686	0
	Protein degradation-Parkin pathway	-0.7039581	0.83516484	1.8072739	0.003731343
	Cell death	1.5957102	0.035128806	2.0140357	0
	Caspase cascades	1.5200465	0.065853655	1.9330438	0.001801802
	Cell death mitochondria pathway	1.6465071	0.029268293	1.6357895	0.016393442

NES, normalized enrichment score; **p-val**, nominal p value.

Acknowledgments

We are grateful to C. Prophete, and P. Ciero for expert technical assistance. We also thank Dr. E. Pamer (Memorial Sloan Kettering Cancer Center) for the generous gift of *Tlr2*^{-/-} and *Tlr4*^{-/-} mice; K. Ireland for assistance in SCD patient study; Z. Chen for the taxonomic microbiota analysis; R. Ng for assistance in GF mice study; O. Uche and G. Wang for assistance in cell sorting; D. Reynolds and W. Tran for the microarray assay; R. Sellers for histopathological analyses. This work was supported by a predoctoral fellowship from American Heart Association (15PRE23010014 to D.Z.) and R01 grants from the National Institutes of Health (HL069438, DK056638, HL116340 to P.S.F). Flow cytometry and cell sorting was supported by a Shared Facilities Award from the New York State Stem Cell Science (NYSTEM) Program.

References

1. Nauseef WM, Borregaard N. Neutrophils at work. *Nature immunology*. 2014; 15:602–611. [PubMed: 24940954]
2. Mayadas TN, Cullere X, Lowell CA. The multifaceted functions of neutrophils. *Annual review of pathology*. 2014; 9:181–218.
3. Taylor PR, et al. Activation of neutrophils by autocrine IL-17A-IL-17RC interactions during fungal infection is regulated by IL-6, IL-23, ROR γ and dectin-2. *Nature immunology*. 2014; 15:143–151. [PubMed: 24362892]
4. Woodfin A, et al. The junctional adhesion molecule JAM-C regulates polarized transendothelial migration of neutrophils in vivo. *Nature immunology*. 2011; 12:761–769. [PubMed: 21706006]
5. Casanova-Acebes M, et al. Rhythmic Modulation of the Hematopoietic Niche through Neutrophil Clearance. *Cell*. 2013; 153:1025–1035. [PubMed: 23706740]
6. Rankin SM. The bone marrow: a site of neutrophil clearance. *Journal of leukocyte biology*. 2010; 88:241–251. [PubMed: 20483920]
7. Martin C, et al. Chemokines acting via CXCR2 and CXCR4 control the release of neutrophils from the bone marrow and their return following senescence. *Immunity*. 2003; 19:583–593. [PubMed: 14563322]
8. Stark MA, et al. Phagocytosis of apoptotic neutrophils regulates granulopoiesis via IL-23 and IL-17. *Immunity*. 2005; 22:285–294. [PubMed: 15780986]
9. Tanji-Matsuba K, et al. Functional changes in aging polymorphonuclear leukocytes. *Circulation*. 1998; 97:91–98. [PubMed: 9443436]
10. Whyte MK, Meagher LC, MacDermot J, Haslett C. Impairment of function in aging neutrophils is associated with apoptosis. *Journal of immunology*. 1993; 150:5124–5134.

11. Hidalgo A, et al. Heterotypic interactions enabled by polarized neutrophil microdomains mediate thromboinflammatory injury. *Nat Med.* 2009; 15:384–391. [PubMed: 19305412]
12. Manwani D, Frenette PS. Vaso-occlusion in sickle cell disease: pathophysiology and novel targeted therapies. *Blood.* 2013; 122:3892–3898. [PubMed: 24052549]
13. Chiang EY, Hidalgo A, Chang J, Frenette PS. Imaging receptor microdomains on leukocyte subsets in live mice. *Nat Methods.* 2007; 4:219–222. [PubMed: 17322889]
14. Turhan A, Weiss LA, Mohandas N, Coller BS, Frenette PS. Primary role for adherent leukocytes in sickle cell vascular occlusion: a new paradigm. *Proc Natl Acad Sci U S A.* 2002; 99:3047–3051. [PubMed: 11880644]
15. Scheiermann C, et al. Adrenergic nerves govern circadian leukocyte recruitment to tissues. *Immunity.* 2012; 37:290–301. [PubMed: 22863835]
16. Gordy C, Pua H, Sempowski GD, He YW. Regulation of steady-state neutrophil homeostasis by macrophages. *Blood.* 2011; 117:618–629. [PubMed: 20980680]
17. Chow A, et al. Bone marrow CD169+ macrophages promote the retention of hematopoietic stem and progenitor cells in the mesenchymal stem cell niche. *The Journal of experimental medicine.* 2011; 208:261–271. [PubMed: 21282381]
18. Subramanian A, et al. Gene set enrichment analysis: a knowledge-based approach for interpreting genome-wide expression profiles. *Proc Natl Acad Sci U S A.* 2005; 102:15545–15550. [PubMed: 16199517]
19. Mortha A, et al. Microbiota-dependent crosstalk between macrophages and ILC3 promotes intestinal homeostasis. *Science.* 2014; 343:1249288. [PubMed: 24625929]
20. Brenchley JM, Douek DC. Microbial translocation across the GI tract. *Annual review of immunology.* 2012; 30:149–173.
21. Khosravi A, et al. Gut microbiota promote hematopoiesis to control bacterial infection. *Cell host & microbe.* 2014; 15:374–381. [PubMed: 24629343]
22. Deshmukh HS, et al. The microbiota regulates neutrophil homeostasis and host resistance to *Escherichia coli* K1 sepsis in neonatal mice. *Nat Med.* 2014; 20:524–530. [PubMed: 24747744]
23. Balmer ML, et al. Microbiota-derived compounds drive steady-state granulopoiesis via MyD88/TICAM signaling. *Journal of immunology.* 2014; 193:5273–5283.
24. Clarke TB, et al. Recognition of peptidoglycan from the microbiota by Nod1 enhances systemic innate immunity. *Nat Med.* 2010; 16:228–231. [PubMed: 20081863]
25. Furze RC, Rankin SM. The role of the bone marrow in neutrophil clearance under homeostatic conditions in the mouse. *FASEB journal: official publication of the Federation of American Societies for Experimental Biology.* 2008; 22:3111–3119. [PubMed: 18509199]
26. Sabroe I, et al. Selective roles for Toll-like receptor (TLR)2 and TLR4 in the regulation of neutrophil activation and life span. *Journal of immunology.* 2003; 170:5268–5275.
27. Magri G, et al. Innate lymphoid cells integrate stromal and immunological signals to enhance antibody production by splenic marginal zone B cells. *Nature immunology.* 2014; 15:354–364. [PubMed: 24562309]
28. Li P, et al. PAD4 is essential for antibacterial innate immunity mediated by neutrophil extracellular traps. *The Journal of experimental medicine.* 2010; 207:1853–1862. [PubMed: 20733033]
29. Chen G, et al. Heme-induced neutrophil extracellular traps contribute to the pathogenesis of sickle cell disease. *Blood.* 2014; 123:3818–3827. [PubMed: 24620350]
30. Gaston MH, et al. Prophylaxis with oral penicillin in children with sickle cell anemia. A randomized trial. *The New England journal of medicine.* 1986; 314:1593–1599. [PubMed: 3086721]
31. Hanoun M, et al. Acute myelogenous leukemia-induced sympathetic neuropathy promotes malignancy in an altered hematopoietic stem cell niche. *Cell stem cell.* 2014; 15:365–375. [PubMed: 25017722]
32. Hang J, et al. 16S rRNA gene pyrosequencing of reference and clinical samples and investigation of the temperature stability of microbiome profiles. *Microbiome.* 2014; 2:31. [PubMed: 25228989]
33. Rothe G, Valet G. Flow cytometric assays of oxidative burst activity in phagocytes. *Methods in enzymology.* 1994; 233:539–548. [PubMed: 8015489]

34. Schnitt SJ, et al. Myocardial fibrin deposition in experimental viral myocarditis that progresses to dilated cardiomyopathy. *Circulation research*. 1993; 72:914–920. [PubMed: 7680288]

Author Manuscript

Author Manuscript

Author Manuscript

Author Manuscript

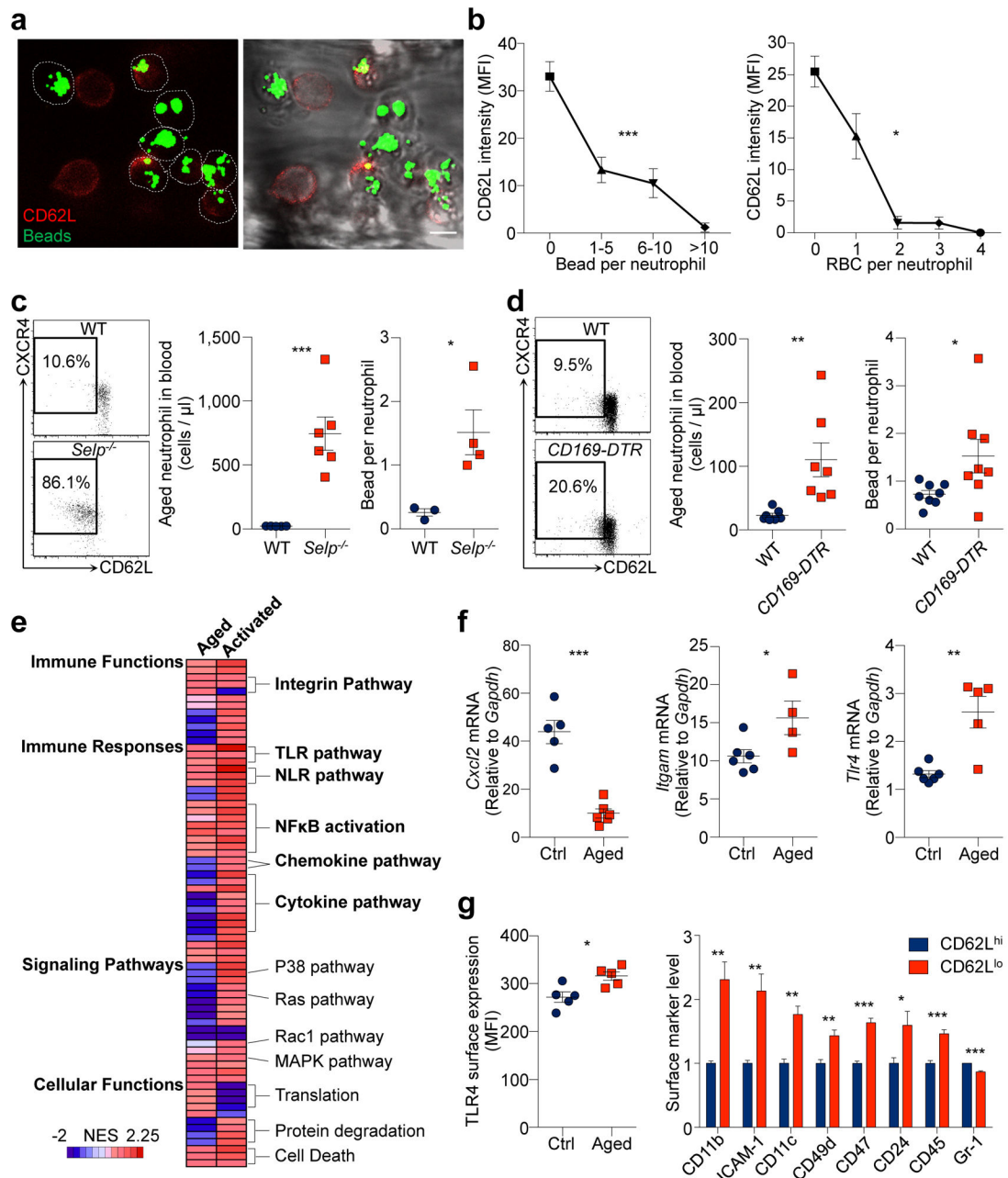


Figure 1. Aged neutrophils represent an overly active subset of neutrophils

a, Multi-channel fluorescence intravital microscopy (MFIM) analysis of CD62L expression (red) and Mac-1 specific albumin-coated fluorescent microsphere beads (green) captured by adherent neutrophils (dashed lines). Left, fluorescence channel; right, fluorescence combined with brightfield channels. Scale bar, 10 μ m. **b**, Correlation between CD62L expression and bead capture or neutrophil-RBC interaction (n = 126 cells from 3 mice). **c-d**, Flow cytometry analysis of CD62L^{lo}CXCR4^{hi} aged neutrophils and MFIM analysis of Mac-1 activation on neutrophils from WT and *Selp*^{-/-} mice (**c**; middle: n = 5,6 mice; right: n = 3,4 mice), or in diphtheria toxin (DT)-treated WT and *CD169-DTR* mice (**d**; middle: n =

7 mice; right: n = 8 mice). **e**, Heat map of normalised enrichment scores (NES) for selected pathways in aged and TNF- α activated neutrophils, as compared to control neutrophils (n = 3 mice). Red, up-regulation; blue, down-regulation. **f–g**, *Cxcl2*, *Itgam*, and *Tlr4* mRNA expression levels by Q-PCR in control and aged neutrophils (**f**; left: n = 5,6 mice; middle: n = 6,4 mice; right: n = 6,5 mice), and surface expression levels of TLR4 and selected adhesion molecules by flow cytometry on CD62L^{lo} aged and CD62L^{hi} young neutrophils (**g**; left: n = 5 mice; right: n = 4 mice). Error bars, mean \pm s.e.m. * $P < 0.05$, ** $P < 0.01$, *** $P < 0.001$, data representing 2 independent experiments analysed with one-way ANOVA (**b**) or unpaired Student's *t*-test (**c**, **d**, **f**, **g**).

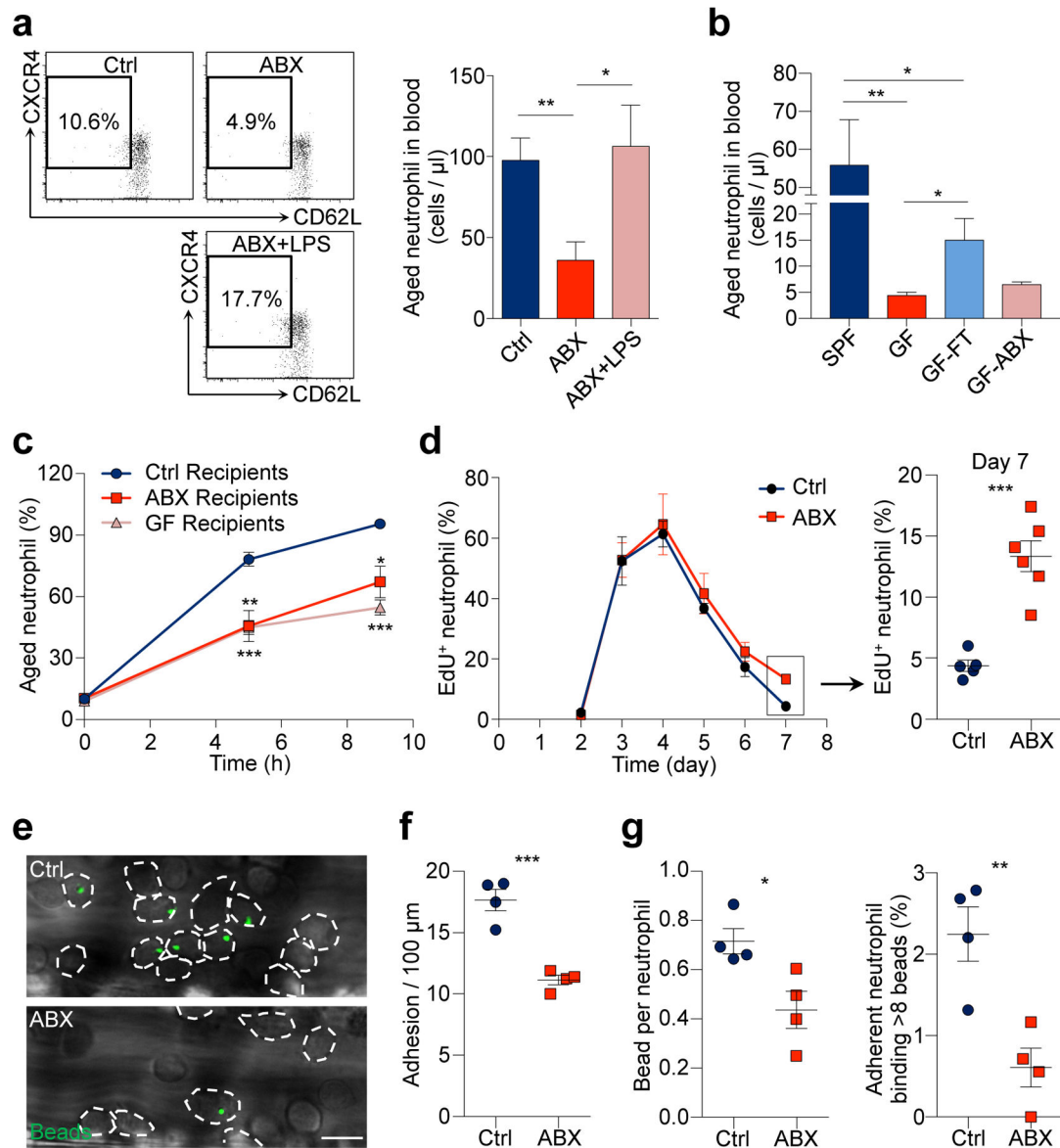


Figure 2. Neutrophil ageing is driven by the microbiota

a, Flow cytometry analysis of aged neutrophils in control, antibiotics (ABX)-treated mice and ABX-treated mice fed with LPS ($n = 12,7,5$ mice). **b**, Numbers of aged neutrophils in specific pathogen free (SPF) mice, Germ-free (GF) mice, GF mice reconstituted by fecal transplantation (GF-FT), and GF mice treated with antibiotics (GF-ABX; $n = 5,5,5,3$ mice). **c**, Ageing kinetics of donor neutrophils after adoptive transfer into control, ABX-treated or GF recipients ($n = 4$ mice). **d**, EdU pulse-chase analysis of neutrophil release-clearance kinetics in control and ABX-treated mice (Ctrl: $n = 5,5,6,8,5$ mice; ABX: $n = 5,5,5,6,6$ mice for day 3,4,5,6,7). **e-g**, Representative images (**e**) and quantification of neutrophil adhesion (dotted lines; **f**) and Mac-1 activation on adherent neutrophils (**g**) in control and ABX-treated mice ($n = 4$ mice). Scale bar, 10 μ m. Error bars, mean \pm s.e.m. * $P < 0.05$, ** $P <$

0.01, *** $P < 0.001$, data representing 2 independent experiments analysed with unpaired Student's *t*-test.

Author Manuscript

Author Manuscript

Author Manuscript

Author Manuscript

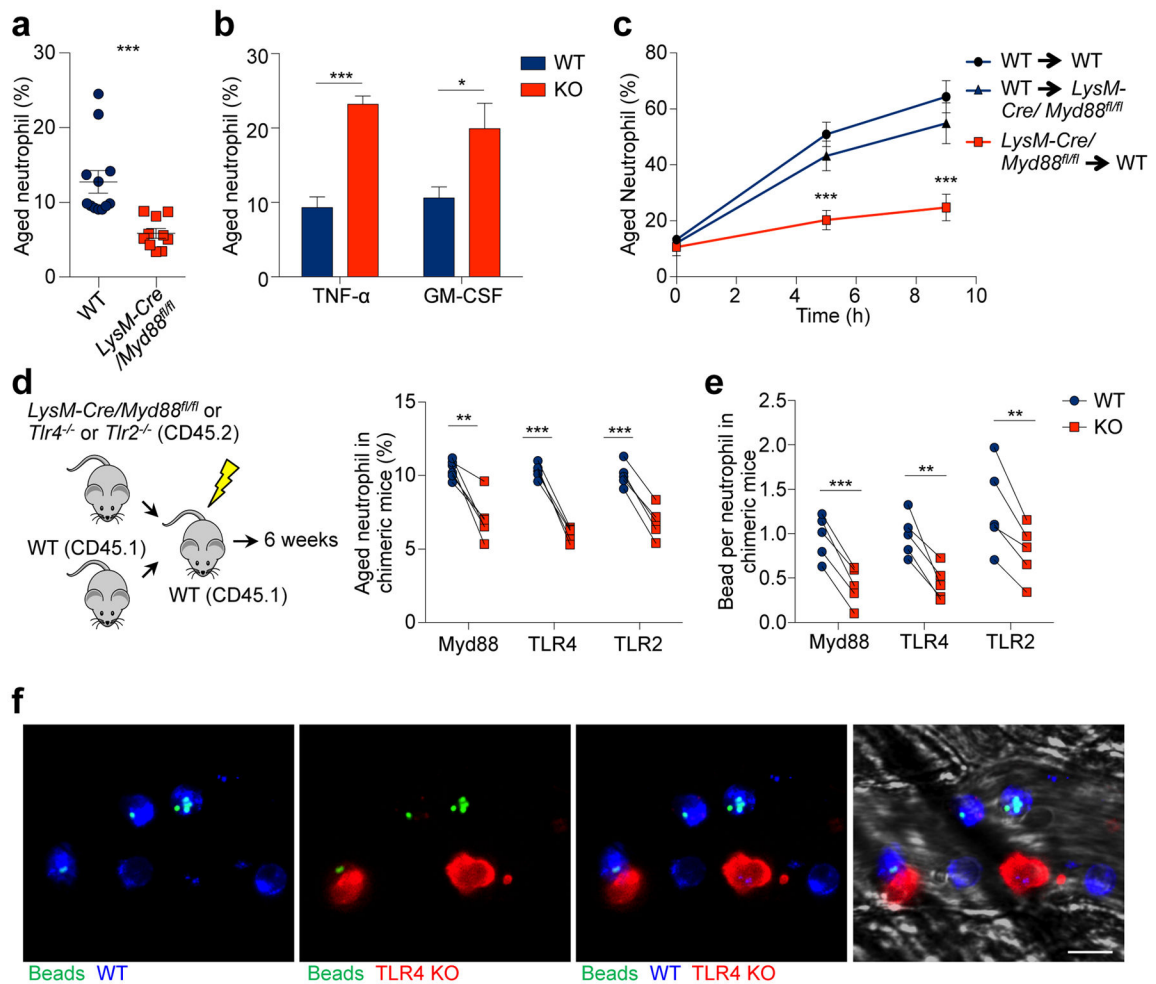


Figure 3. Microbiota-driven neutrophil ageing is mediated by neutrophil TLRs and Myd88 signalling

a, Percentages of aged neutrophils in WT and *LysM-cre/Myd88^{fl/fl}* mice, as analysed by flow cytometry (n = 12,10 mice). **b**, Percentages of aged neutrophils in WT and *Tnf^{-/-}* or *Csf2^{-/-}* mice (n = 5 mice). **c**, Ageing kinetics of donor neutrophils after adoptive transfer from either WT or *LysM-cre/Myd88^{fl/fl}* mice into WT or *LysM-cre/Myd88^{fl/fl}* recipients (n = 6 mice). **d**, Percentages of the aged subset in WT and *LysM-cre/Myd88^{fl/fl}*, *Tlr4^{-/-}* or *Tlr2^{-/-}* neutrophils in chimeric mice (n = 5 mice). **e**, MFIM analysis of Mac-1 activation on WT and *LysM-cre/Myd88^{fl/fl}*, *Tlr4^{-/-}* or *Tlr2^{-/-}* neutrophils in chimeric mice (n = 5 mice). **f**, Representative images showing WT (CD45.1⁺, blue) and *Tlr4^{-/-}* (CD45.2⁺, red) neutrophils and beads (green) captured. Scale bar, 10 μ m. Error bars, mean \pm s.e.m. * $P < 0.05$, ** $P < 0.01$, *** $P < 0.001$, data representing 2 independent experiments analysed with unpaired Student's *t*-test (**a-c**) or paired Student's *t*-test (**d-e**).

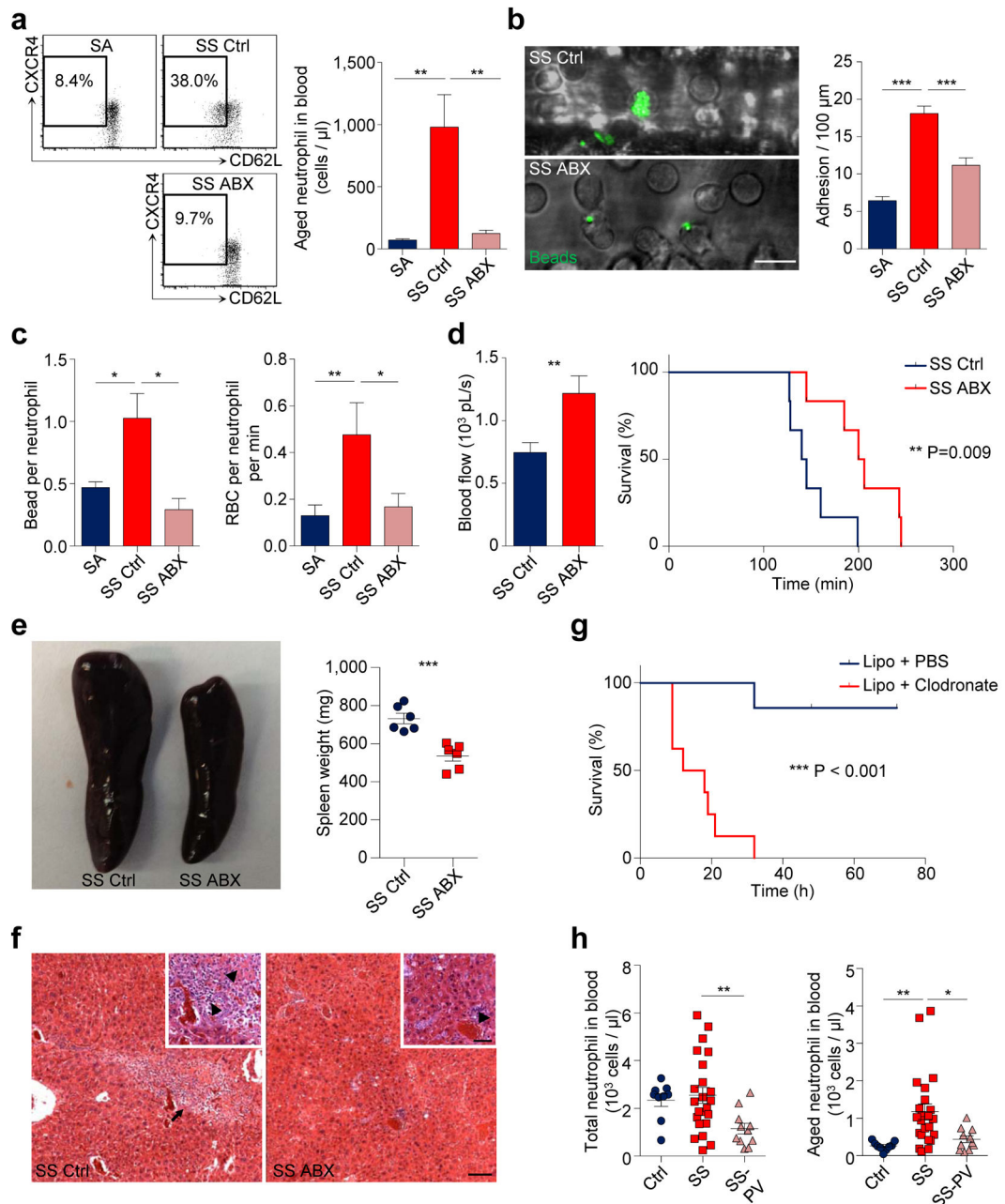


Figure 4. Microbiota depletion reduces vaso-occlusive events in sickle cell disease

a, Flow cytometry analysis of aged neutrophils in hemizygous control (SA), control SCD (SS Ctrl) and antibiotics-treated SCD (SS ABX) mice ($n = 8,9,9$ mice). **b**, MFIM analysis of neutrophil adhesion and Mac-1 activation on adherent neutrophils in SA, SS Ctrl and SS ABX mice ($n = 6,8,10$ mice). Scale bar, 10 μm . **c**, Mac-1 activation on adherent neutrophils and neutrophil-RBC interaction in SA, SS Ctrl and SS ABX mice (left, $n = 4,3,3$ mice; right, $n = 69,42,54$ vessels from 6,7,7 mice). **d**, Blood flow and survival time of SS Ctrl and SS ABX mice in acute vaso-occlusive crisis (left, $n = 36,48$ vessels from 7,8 mice; right, $n = 6$ mice). **e**, Representative images and weights of spleen in SS Ctrl and SS ABX mice ($n = 6$

mice). **f**, Hematoxylin and eosin (H&E) staining showing liver damage in SS Ctrl and SS ABX mice. Arrow, liver fibrosis; arrowheads, necrosis and inflammation. Scale bars, 50 μm . **g**, Survival time of SS mice treated with PBS- or clodronate-encapsulated liposome (n = 7,8 mice). **h**, Numbers of total and aged neutrophils in healthy controls, SCD patients (SS), and SCD patients on penicillin V prophylaxis (SS-PV; n = 9,23,11 subjects). Error bars, mean \pm s.e.m. * $P < 0.05$, ** $P < 0.01$, *** $P < 0.001$, data representing 2 independent experiments analysed with unpaired Student's *t*-test (**a–d**(left), **e, h**) or *Log-rank* test (**d**(right), **g**).